

FEB 20 1953

CLASSIFICATION CHANGED

~~CONFIDENTIAL~~
~~SECURITY INFORMATION~~

~~RESTRICTED~~

SECURITY INFORMATION

~~CONFIDENTIAL~~

By authority of *H. H. Snyder per NACA memo*
Form 1395- 4/10/53 Date 2/20/53

RESEARCH MEMORANDUM

TESTS IN THE AMES 40- BY 80-FOOT WIND TUNNEL OF TWO
AIRPLANE MODELS HAVING ASPECT RATIO 2 TRAPEZOIDAL
WINGS OF TAPER RATIOS 0.33 AND 0.20

By Ralph W. Franks

Ames Aeronautical Laboratory
Moffett Field, Calif.

CLASSIFICATION CHANGED

To

Confidential

Release form # 1422

By authority of *J. H. Crawley* Date *12/1/53*

This material contains information affecting the National Defense of the United States within the meaning of the espionage laws, Title 18, U.S.C., Secs. 793 and 794, the transmission or revelation of which in any manner to an unauthorized person is prohibited by law.

NATIONAL ADVISORY COMMITTEE FOR AERONAUTICS

WASHINGTON

February 16, 1953

~~CONFIDENTIAL~~

~~SECURITY INFORMATION~~ ~~CONFIDENTIAL~~

NACA LIBRARY
LANGLEY AERONAUTICAL LABORATORY
Langley Field, Va.

CLASSIFICATION CANCELLED

Authority *NACA-RA 644*
RAN 20 94
By *SADTA 1116756*
Date *12/4/53*
Sec *12/4/53*



NATIONAL ADVISORY COMMITTEE FOR AERONAUTICS

RESEARCH MEMORANDUM

TESTS IN THE AMES 40- BY 80-FOOT WIND TUNNEL OF TWO
AIRPLANE MODELS HAVING ASPECT RATIO 2 TRAPEZOIDAL
WINGS OF TAPER RATIOS 0.33 AND 0.20

By Ralph W. Franks

SUMMARY

Tests have been made of two airplane models having trapezoidal wings of aspect ratio 2 and taper ratios of 0.33 and 0.20. For each model, a fuselage with a fineness ratio of 12.5, a thin, triangular, vertical tail with a constant-chord rudder, and a thin, unswept, all-movable horizontal tail was used. The wings had an NACA 0005 modified section and were equipped with slotted, trailing-edge flaps. Tests of the wing-fuselage vertical-tail configuration and of the complete airplane model were made for both models. Tests were made with the horizontal tail at each of three vertical locations. The flaps were tested as high-lift and lateral-control devices. When mounted on the model having a wing of taper ratio 0.33, the horizontal tail was tested as a lateral control by giving the two surfaces antisymmetric deflections. The Reynolds numbers, based on the wing mean aerodynamic chord, were approximately 11.4 and 13.0 million for the taper ratios 0.33 and 0.20 wings, respectively. The Mach number was approximately 0.13. No analysis is made of the data presented.

INTRODUCTION

The low-speed aerodynamic characteristics of triangular-wing airplane models having wings of aspect ratios 2, 3, and 4 have been under investigation in the Ames 40- by 80-foot wind tunnel, and results have been reported in references 1, 2, and 3. Interest has been expressed in the aerodynamic characteristics of these wings when the plan form was modified by the removal of the pointed tips. As a result of this interest, tests were carried out on the aspect ratios 3 and 4

~~CONFIDENTIAL~~
~~RESTRICTED~~
SECURITY INFORMATION

triangular-wing models with the wing plan forms modified to form trapezoidal wings of aspect ratio 2 and taper ratios of 0.20 and 0.33, respectively.

Tests were made to ascertain the effectiveness of a high-lift device, two types of lateral controls, and a directional control, using control-surface deflections typical of those used in landing. The horizontal tail was tested in three vertical locations in order to determine the effect of horizontal-tail vertical location on the longitudinal stability. The wings of both models had slotted, trailing-edge flaps which were tested both as high-lift devices and lateral controls. An all-movable horizontal tail was tested as a longitudinal control on both models, and as a lateral control on one of the models. A rudder of constant chord was tested as a directional control on one model. The data are presented without analysis to expedite publication.

NOTATION

The sign convention for force and moment coefficients, angles, and control deflections is shown in figure 1. All control deflections are measured in a plane perpendicular to the control hinge line. The coefficients and symbols used in this report are defined as follows:

- α angle of attack of the wing-chord plane with reference to free stream, deg
- b wing span, ft
- b_f flap span (total movable), ft
- b_t horizontal-tail span, ft
- c wing chord (measured parallel to wing center line), ft
- \bar{c} mean aerodynamic chord of wing (measured parallel to wing center line), $\frac{\int_0^{b/2} c^2 dy}{\int_0^{b/2} c dy}$, ft
- c_f flap chord (measured parallel to wing center line), ft
- C_D drag coefficient, drag/ qS

- C_l rolling-moment coefficient, rolling moment/ qSb
- C_L lift coefficient, lift/ qS
- C_m pitching-moment coefficient, pitching moment/ qSc
- C_n yawing-moment coefficient, yawing moment/ qSb
- C_Y side-force coefficient, side force/ qS
- δ_f average of the right and left flap deflections, deg
- δ_l difference in deflection between any pair of control surfaces used as lateral controls; positive when left-hand surface has the more positive deflection, deg (Subscripts denote the control used: f, flaps; t, horizontal tail.)
- δ_r rudder deflection, deg
- Δ prefix denoting an increment
- ϵ_{av} average effective downwash angle, deg
- i_t average of the right and left horizontal-tail incidences relative to the wing-chord plane, deg
- l_t distance from moment center of model to pivot line of horizontal tail, ft
- L/D lift-drag ratio
- λ wing taper ratio, tip chord/root chord
- q free-stream dynamic pressure, lb/sq ft
- S wing area, sq ft
- S_f flap area (total movable), sq ft
- S_r rudder area (total movable), sq ft
- S_t horizontal-tail area (total movable), sq ft
- S_v vertical-tail area (total exposed), sq ft

- V free-stream velocity, ft/sec
- W airplane weight, lb
- x longitudinal coordinate parallel to model center line, ft
- y lateral coordinate perpendicular to plane of symmetry, ft
- z vertical coordinate perpendicular to wing-chord plane, ft

DESCRIPTION OF MODEL

Drawings of the complete airplane models are shown in figures 2 and 3, and pertinent dimensional data are presented in table I. Photographs of the models as mounted in the Ames 40- by 80-foot wind tunnel are shown in figure 4.

The airfoil sections of both wings, taken parallel to the model center line, were NACA 0005 sections modified by using a straight-line fairing from the 67-percent-chord station to the trailing edge. A further modification to the portion of the wing having a taper ratio of 0.20 shown in figure 5 consisted of a smooth fairing made necessary because of the construction technique used. The deviation of this modified fairing from the actual NACA 0005 profile did not exceed 0.1-percent chord.

The dimensions of the fuselage are given in table I. The fuselage was of circular cross section and had a fineness ratio of 12.5. Fuselage coordinates are given in reference 1.

The vertical tail had a triangular plan form with modified NACA 0005 airfoil sections (streamwise) and was equipped with a constant-chord rudder. The rudder had a plain radius nose and a small unsealed gap.

The horizontal tail had an unswept plan form and modified diamond airfoil sections. The original section of 5.6-percent thickness was modified by rounding the maximum-thickness ridge using a radius of curvature of 4.48 chord; the resulting section had a maximum thickness of 4.2-percent chord. The three vertical locations of the horizontal tail above the extended wing-chord plane are given in table I.

The trailing-edge flaps were of the slotted type and were of constant chord. Details of the flaps and their path of travel are shown in figure 6.

TESTS AND PROCEDURE

The configurations tested are listed in table II. The flaps were tested as lateral-control surfaces by deflecting these surfaces anti-symmetrically, the deflections being superposed on initial symmetrical settings.

The horizontal tail was tested as a lateral control in the same manner; however, tests were made only for the model having a wing of taper ratio 0.33 because the results were thought to be representative of those which would be obtained by corresponding tests of the model having a wing of taper ratio 0.20. Tests were also made with the rudder of the model having a wing of taper ratio 0.33 deflected to ascertain rudder effectiveness and to study possible control interaction between the rudder and horizontal tail when the tail was used as a lateral control.

The data were corrected for wind-tunnel-wall effects using the method of reference 4. The data were also corrected for support-strut interference. No corrections were applied to the data for possible deflection of the control surfaces due to aerodynamic loads since they were believed to be negligible. The accuracy of setting of all control-surface deflections was within $\pm 0.2^\circ$. The average Reynolds number of the tests, based on the wing mean aerodynamic chord, was 11.4 and 13.0 million for the taper ratio 0.33 and 0.20 wings, respectively. The average test dynamic pressure was 25 pounds per square foot and the Mach number was approximately 0.13.

RESULTS

The basic experimental data obtained are presented in figures 7 to 19, which are indexed in table II. A center-of-gravity position at 25 percent of the mean aerodynamic chord was used as a moment center for the data presented in figure 7. For the data presented in the remainder of the figures, a moment center was selected which would give a static margin of 6 percent, $[(dC_m/dC_L)_{C_{L=0}} = -0.06]$ for the model with control surfaces undeflected and with the horizontal tail on. The center-of-gravity locations used as moment centers are tabulated in table III.

The increments of lift coefficient obtained by deflecting the flaps to 40° on the wing-fuselage vertical-tail configurations at zero angle of attack are plotted in figure 20 against the increments predicted by the theory described in reference 5.

The trimmed lift and drag characteristics for the models are shown in figure 21. The trimmed data are shown only for the models having the horizontal tail in the low position, since locating the tail in either the middle or high positions results in poor longitudinal stability. Curves of constant gliding and sinking speeds, based on a wing loading of 30 pounds per square foot, are included in the figure.

The effect of vertical location of the horizontal tail on the longitudinal-stability characteristics of the models with flaps undeflected are summarized in figure 22. Figure 23 shows the variation of the average effective downwash with angle of attack at the various positions of the horizontal tail for the models with flaps undeflected. The downwash variation with angle of attack with the flaps deflected to 40° is shown in figure 24 for the low position only. The downwash angles were determined from the test data by making the assumption that for any given tail incidence, the intersection of the tail-on and the tail-off pitching-moment curves indicates the lift-coefficient value at which the pitching moment due to the tail is zero; hence, the average angle of flow across the tail is zero. Under this condition, ϵ_{av} equals $\alpha + i_t$. In order to obtain points of intersection for tail incidences other than those tested, a linear variation of dC_m/di_t was assumed.

The lateral-control data are summarized in figures 25 to 27. The effectiveness of the flaps in producing rolling moment is shown in figures 25 and 26. The effectiveness of the horizontal tail as a lateral control is shown in figure 27. The results are compared with the values obtained from the theory given in reference 6.

The increments of C_l , C_n , and C_y per degree of rudder deflection, as measured with $\delta_F = 40^\circ$, are presented in figure 28. This figure also shows the effect of use of the horizontal tail as a lateral-control device on the rudder effectiveness.

Ames Aeronautical Laboratory
National Advisory Committee for Aeronautics
Moffett Field, Calif.

REFERENCES

1. Graham, David, and Koenig, David G.: Tests in the Ames 40- by 80-Foot Wind Tunnel of an Airplane Configuration With an Aspect Ratio 4 Triangular Wing and an All-Movable Horizontal Tail - Longitudinal Characteristics. NACA RM A51H10a, 1951.
2. Koenig, David G.: Tests in the Ames 40- by 80-Foot Wind Tunnel of an Airplane Configuration With an Aspect Ratio 3 Triangular Wing and an All-Movable Horizontal Tail - Longitudinal and Lateral Characteristics. NACA RM A52L15, 1953.
3. Franks, Ralph W.: Tests in the Ames 40- by 80-Foot Wind Tunnel of an Airplane Model With an Aspect Ratio 4 Triangular Wing and an All-Movable Horizontal Tail - High-Lift Devices and Lateral Controls. NACA RM A52K13, 1953.
4. Tani, Itiro, and Sanuki, Matao: The Wall Interference of a Wind Tunnel of Elliptic Cross Section. NACA TM 1075, 1944.
5. DeYoung, John: Theoretical Symmetric Span Loading Due to Flap Deflection for Wings of Arbitrary Plan Form at Subsonic Speeds. NACA Rep. 1071, 1951. (Supersedes NACA TN 2278)
6. DeYoung, John: Theoretical Antisymmetric Span Loading for Wings of Arbitrary Plan Form at Subsonic Speeds. NACA Rep. 1056, 1950. (Supersedes NACA TN 2140)

TABLE I.- DIMENSIONAL DATA

	Wing Taper Ratio	
	0.33	0.20
Wing		
Area, sq ft	277.8	301.2
Span, ft	23.56	24.52
Mean aerodynamic chord, ft	12.77	14.11
Aspect ratio	2.0	2.0
Sweep, quarter-chord line, deg	36.87	45.00
Slotted, trailing-edge flaps		
S_f/S	0.135	0.124
b_f/b	0.809	0.778
c_f/\bar{c}	0.154	0.139
Fuselage		
Length, ft	56.16	56.16
Maximum diameter, ft	4.49	4.49
Fineness ratio	12.50	12.50
Vertical tail		
S_v/S	0.189	0.174
S_r/S_v	0.245	0.245
Rudder chord, ft	1.76	1.76
Aspect ratio of plan form extended to model center line	1.0	1.0
Taper ratio	0	0
Horizontal tail		
Low position		
S_t/S	0.277	0.255
b_t/b	0.782	0.751
l_t/\bar{c}	1.716	1.585
$z/(b/2)$	0	0
Aspect ratio	4.4	4.4
Taper ratio	0.46	0.46

TABLE I.- DIMENSIONAL DATA - Concluded

	Wing Taper Ratio	
	0.33	0.20
Horizontal tail (continued)		
Middle position		
S_t/S	0.225	0.207
b_t/b	0.671	0.645
l_t/\bar{c}	1.682	1.554
$z/(b/2)$	0.269	0.259
Aspect ratio	4.0	4.0
Taper ratio	0.50	0.50
High position		
S_t/S	0.225	0.207
b_t/b	0.671	0.645
l_t/\bar{c}	1.603	1.497
$z/(b/2)$	0.537	0.516
Aspect ratio	4.0	4.0
Taper ratio	0.50	0.50



TABLE II.- SUMMARY OF CONFIGURATIONS TESTED
 [W, wing; F, fuselage; V, vertical tail; H, horizontal tail.
 (Subscripts denote horizontal-tail location: L, low;
 M, middle; H, high)]

Figure no.	Configurations	Wing taper ratio	Control deflections, deg					α , deg
			Flaps		Horizontal tail		Rudder	
			δ_f	δ_{lf}	1_t	δ_{lt}	δ_r	
7	W+F+V	0.33, 0.20	0 40	0	---	---	0	-2 → 26
8	W+F+V+H _L	0.33	0	0	0 -2 -6 -10	0	0	-2 → 25
	W+F+V	0.33	0	0	---	0	0	
9	W+F+V+H _L	0.20	0	0	0 -2 -6 -10	0	0	-2 → 26
	W+F+V	0.20	0	0	---	0	0	
10	W+F+V+H _L	0.33	40	0	0 -2 -6 -10	0	0	-2 → 26
	W+F+V	0.33	40	0	---	0	0	
11	W+F+V+H _L	0.20	40	0	0 -2 -6 -10	0	0	-2 → 26
	W+F+V	0.20	40	0	---	0	0	
12	W+F+V+H _M	0.33	0	0	0 -2 -6	0	0	-2 → 25
	W+F+V	0.33	0	0	---	0	0	
13	W+F+V+H _M	0.20	0	0	0 -2 -6	0	0	-2 → 26
	W+F+V	0.20	0	0	---	0	0	
14	W+F+V+H _H	0.33	0	0	0 -2 -6	0	0	-2 → 25
	W+F+V	0.33	0	0	---	0	0	
15	W+F+V+H _H	0.20	0	0	0 -1.5 -6	0	0	-2 → 26
	W+F+V	0.20	0	0	---	0	0	
16	W+F+V+H _L	0.33	0 30	20	-10	0	0	-2 → 26
	W+F+V	0.33	0 30	20	---	0	0	
17	W+F+V+H _L	0.20	0 30	20	-6	0	0	-2 → 26
	W+F+V	0.20	0 30	20	---	0	0	
18	W+F+V+H _L	0.33	0 40	0	-10	20	0	-2 → 25
19	W+F+V+H _L	0.33	40	0	-10	0 10 20	10	-2 → 26

NACA

TABLE III.- CENTER-OF-GRAVITY LONGITUDINAL LOCATIONS
FOR THE VARIOUS CONFIGURATIONS

Tail position	Center-of-gravity location on fuselage center line (fraction \bar{c})	
	Taper ratio 0.33	Taper ratio 0.20
Low	0.338	0.369
Middle	.372	.400
High	.451	.457

NACA

[REDACTED]

[REDACTED]

[REDACTED]

Note: All force and moment coefficients, angles, and control-surface deflections are shown as positive.

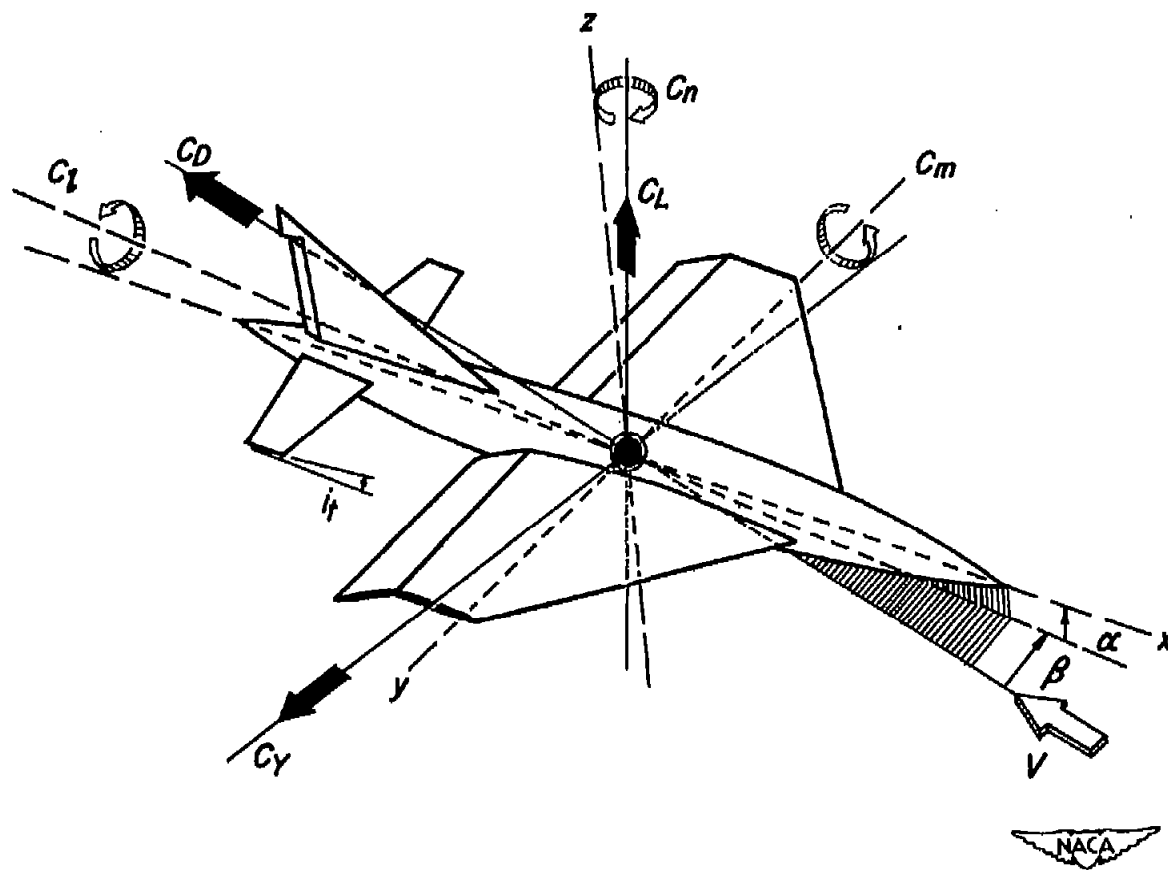


Figure 1.— Sign convention for force and moment coefficients.

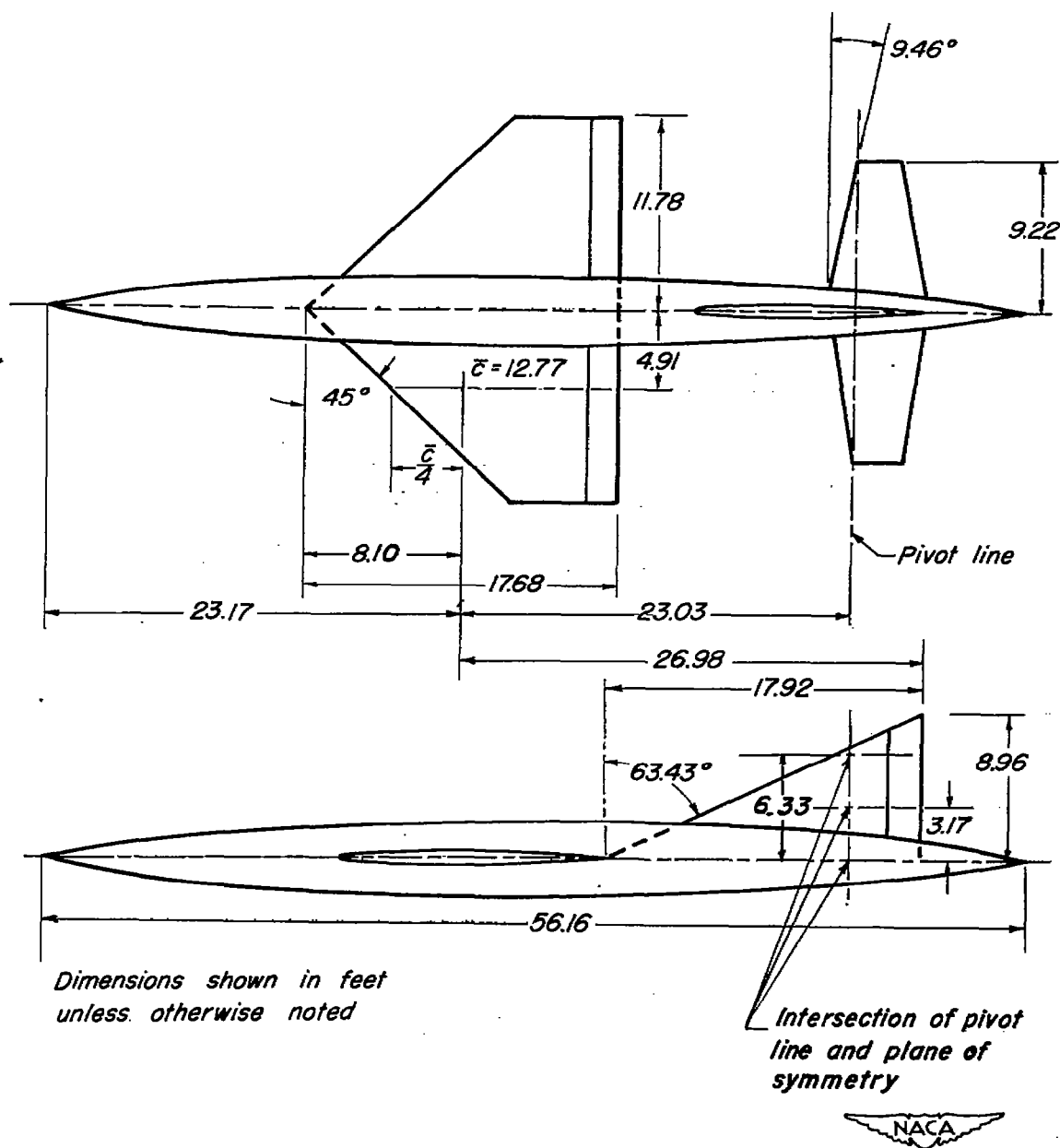


Figure 2.— Geometric details of the model with the wing of taper ratio 0.33.

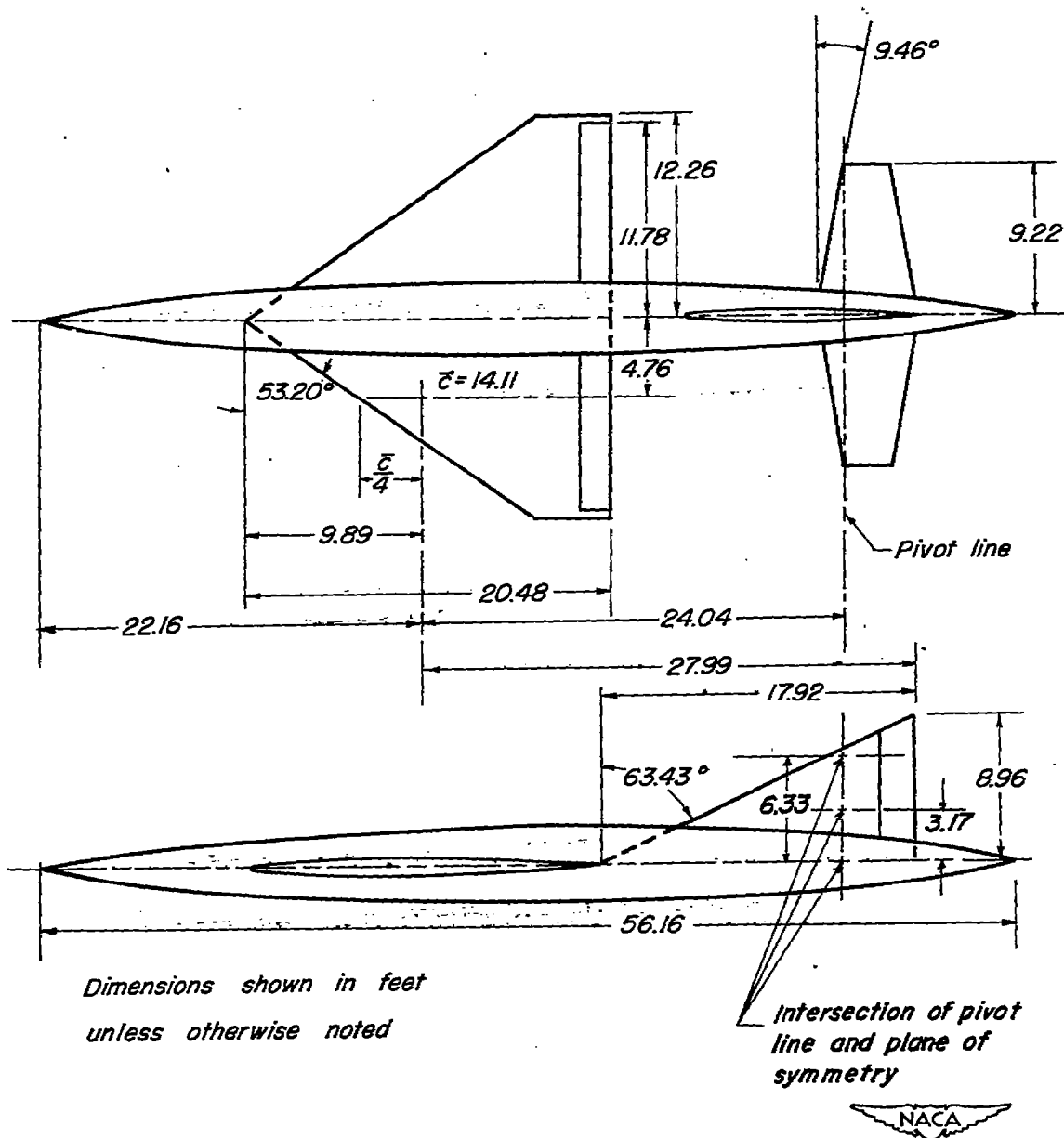
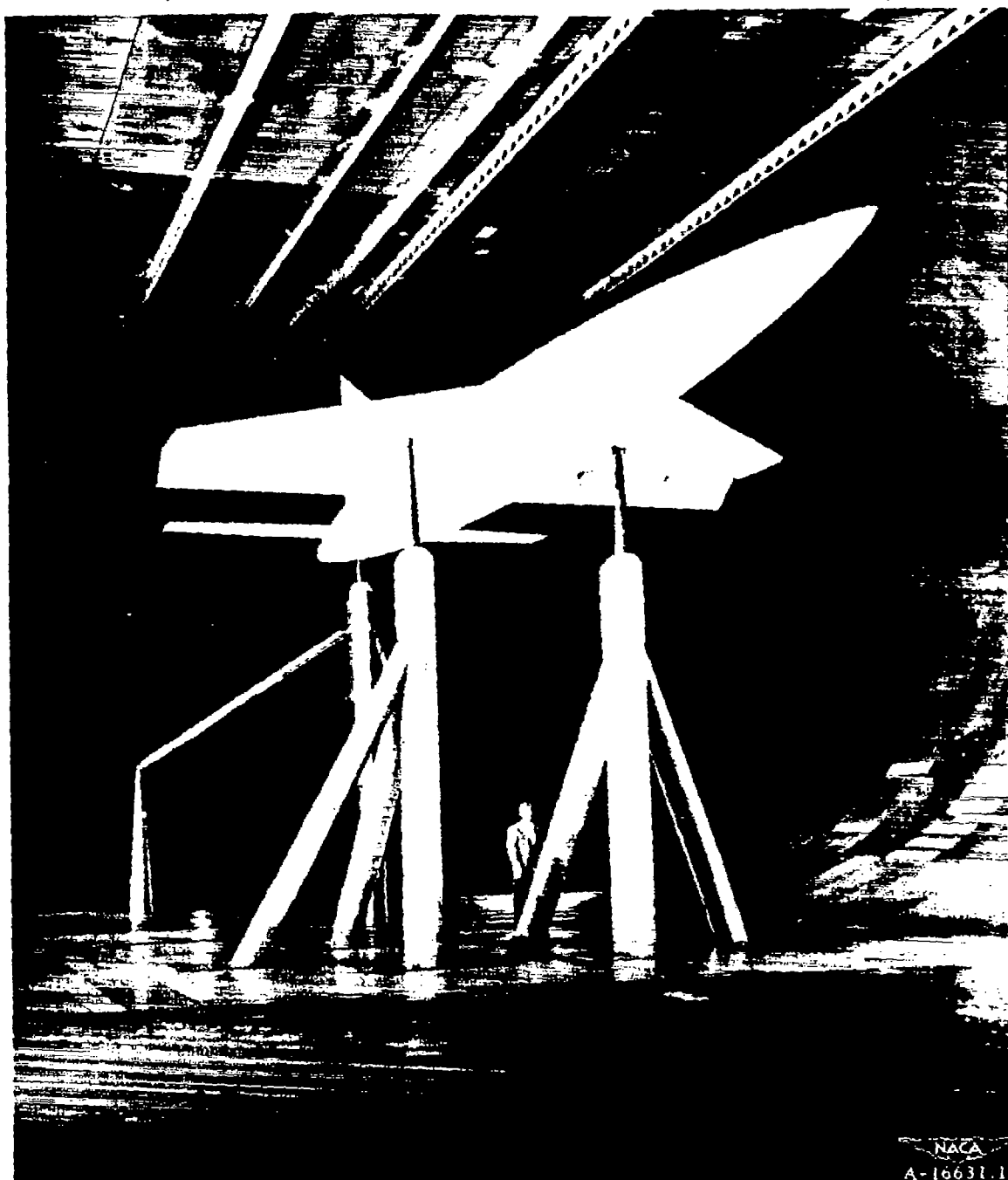
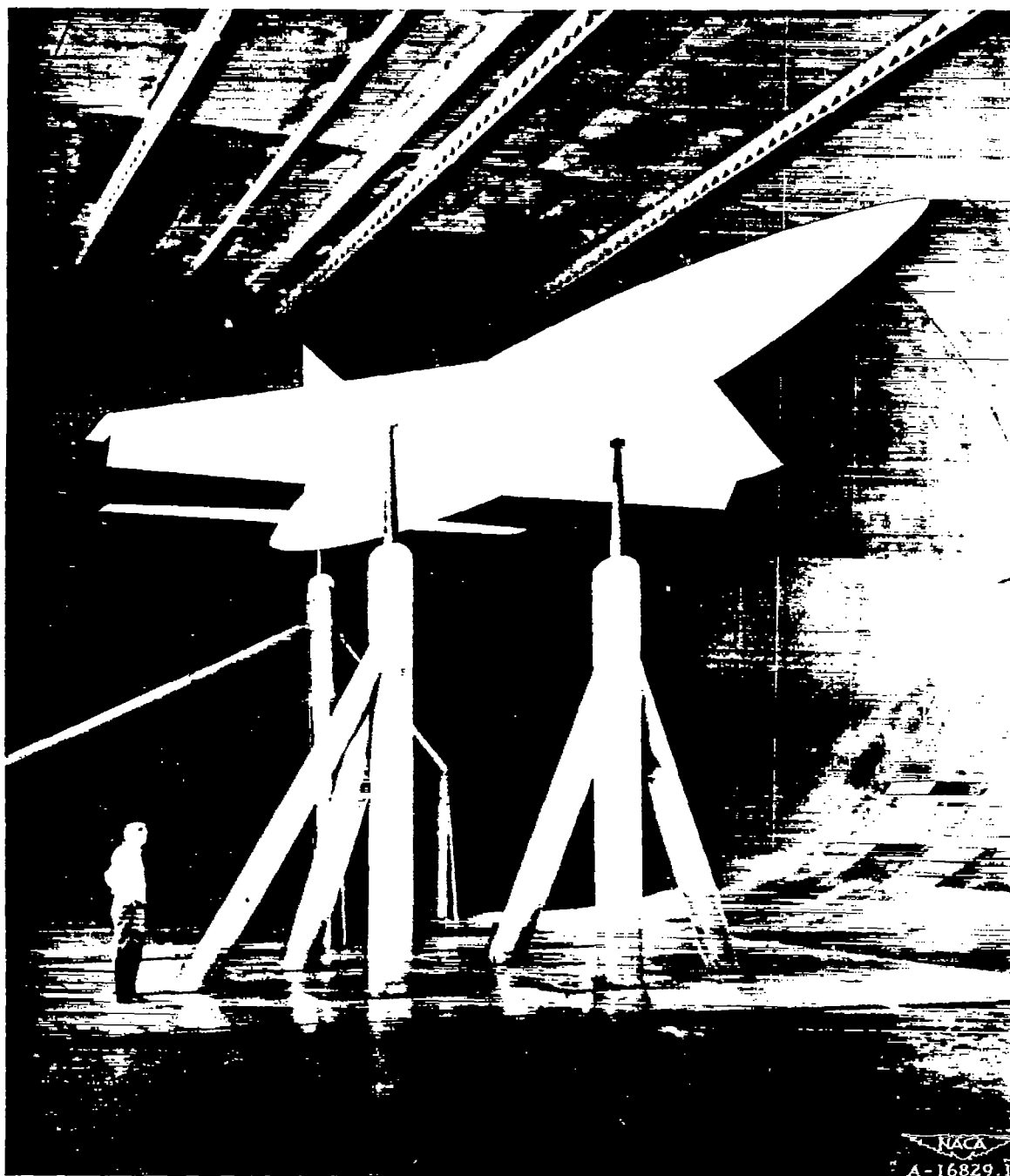


Figure 3.— Geometric details of the model with the wing of taper ratio 0.20.



(a) Model with a wing of taper ratio 0.33.

Figure 4.— Photograph of the models as mounted in the Ames
40- by 80-foot wind tunnel.



(b) Model with a wing of taper ratio 0.20.

Figure 4.- Concluded.

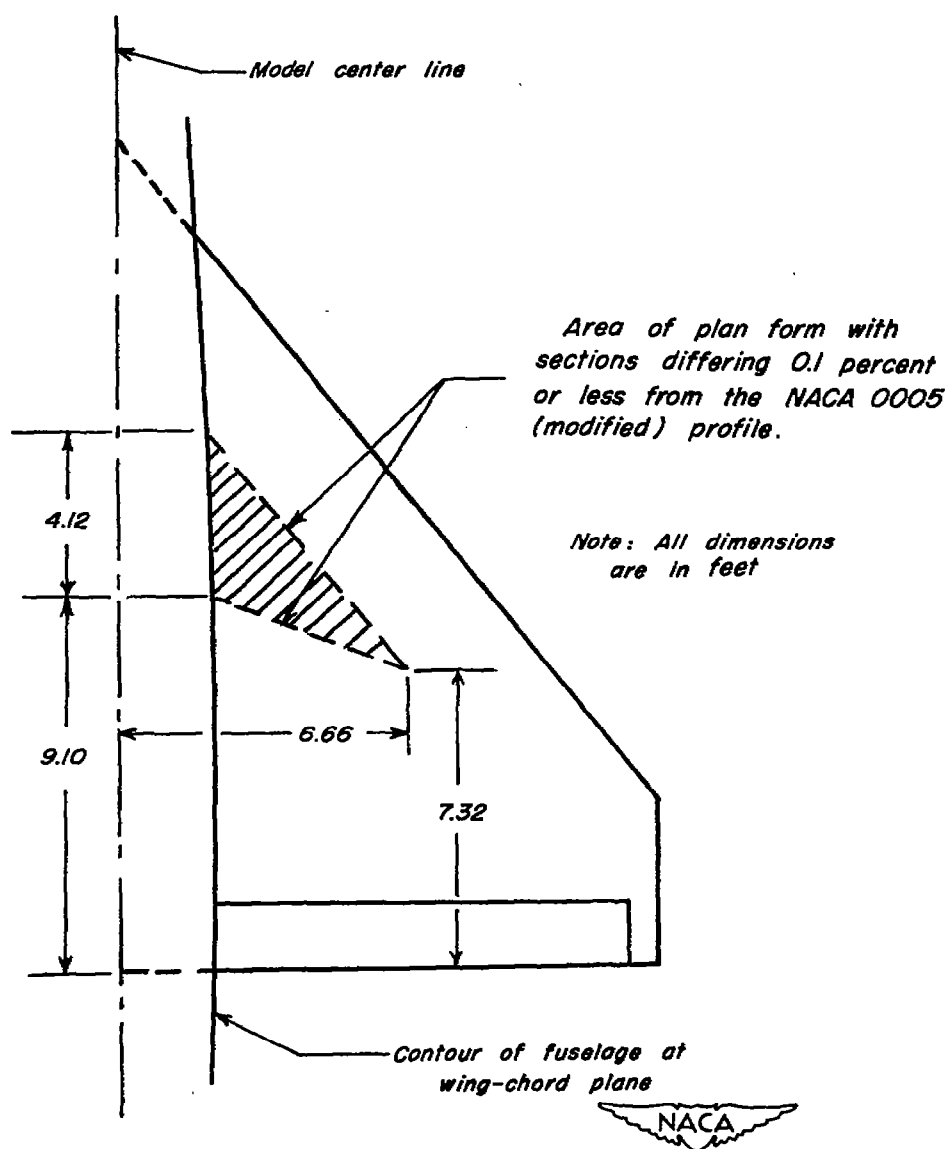
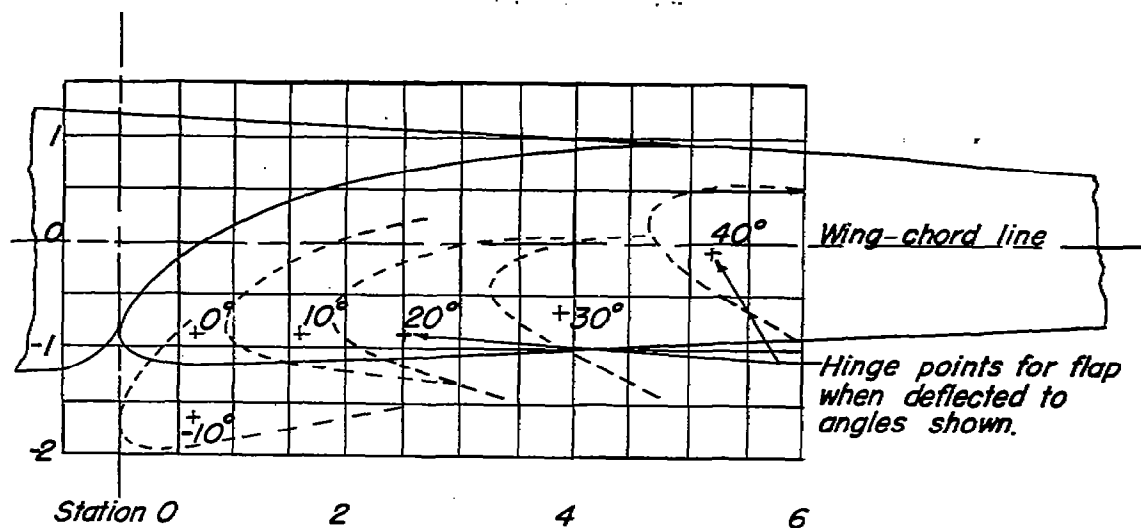


Figure 5.— Area of wing of taper ratio 0.20 having airfoil sections deviating from those used for the wing of taper ratio 0.33.

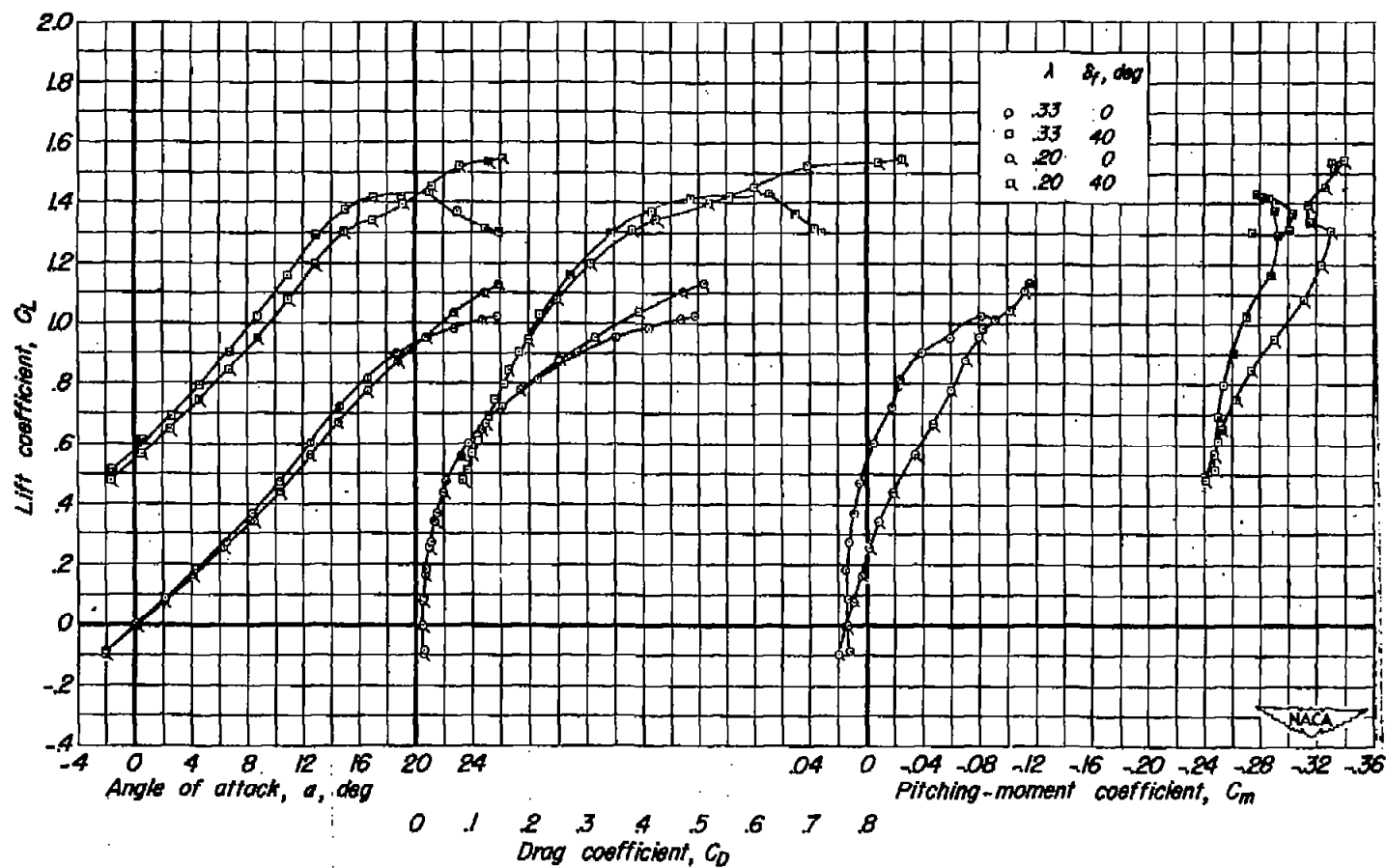


Flap coordinates		
Station	Upper surface	Lower surface
0	-0.872	-0.872
0.113	- .554	- 1.030
.226	- .408	- 1.086
.452	- .181	- 1.119
.679	- .012	- 1.131
1.357	.351	- 1.119
2.036	.589	- 1.086
2.714	.747	- 1.041
3.393	.860	- 1.006
4.071	.905	- 0.973
4.750	.916	- 0.938
5.654	.905	- 0.905
11.309	.610	- 0.610
16.963	.328	- 0.328
23.560	0	0
Center of L.E. arc		
0.17	-0.87	
L.E. radius: 0.17		

Dimensions shown
in inches.

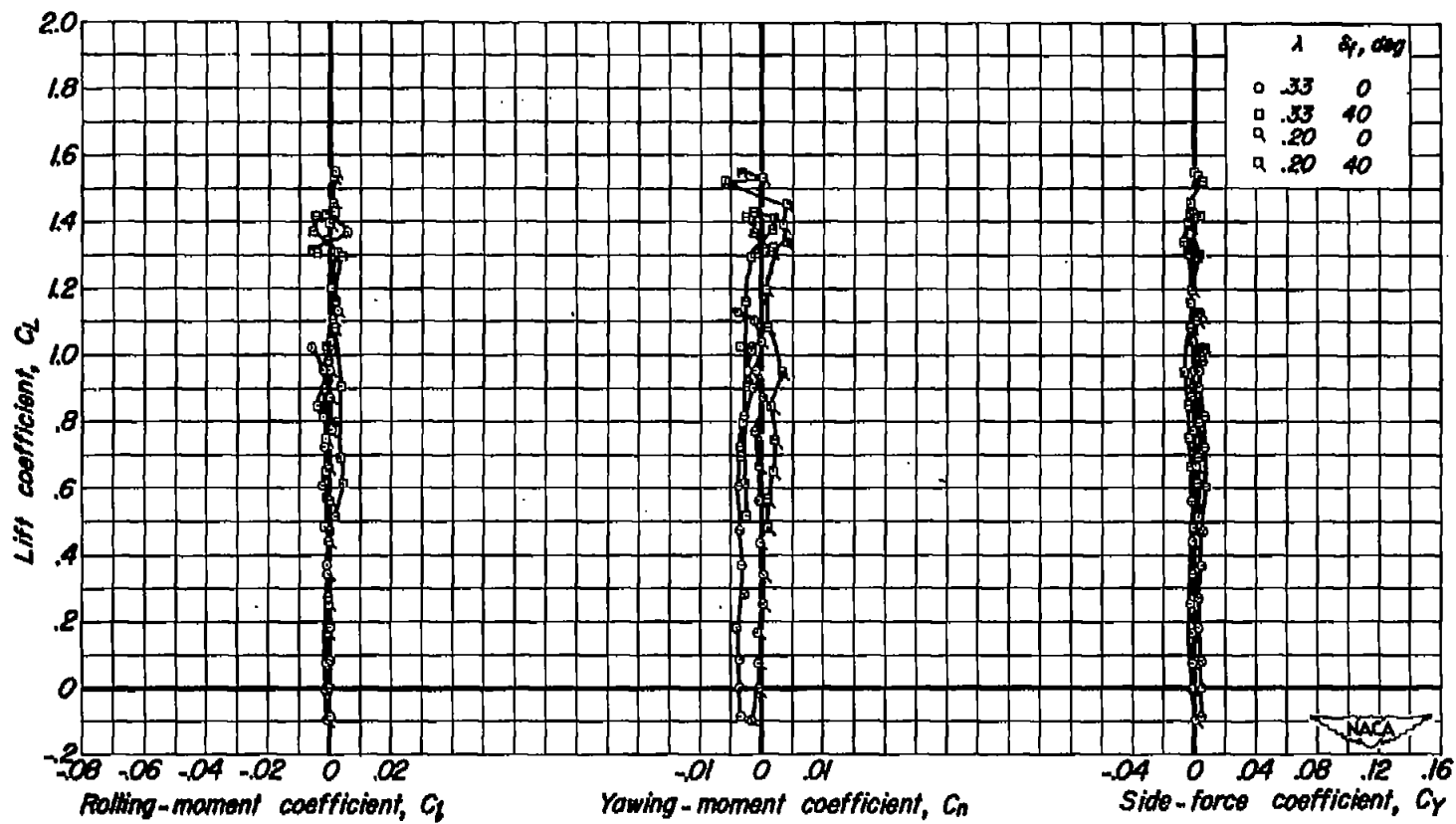


Figure 6.— Details of the slotted, trailing-edge flaps.



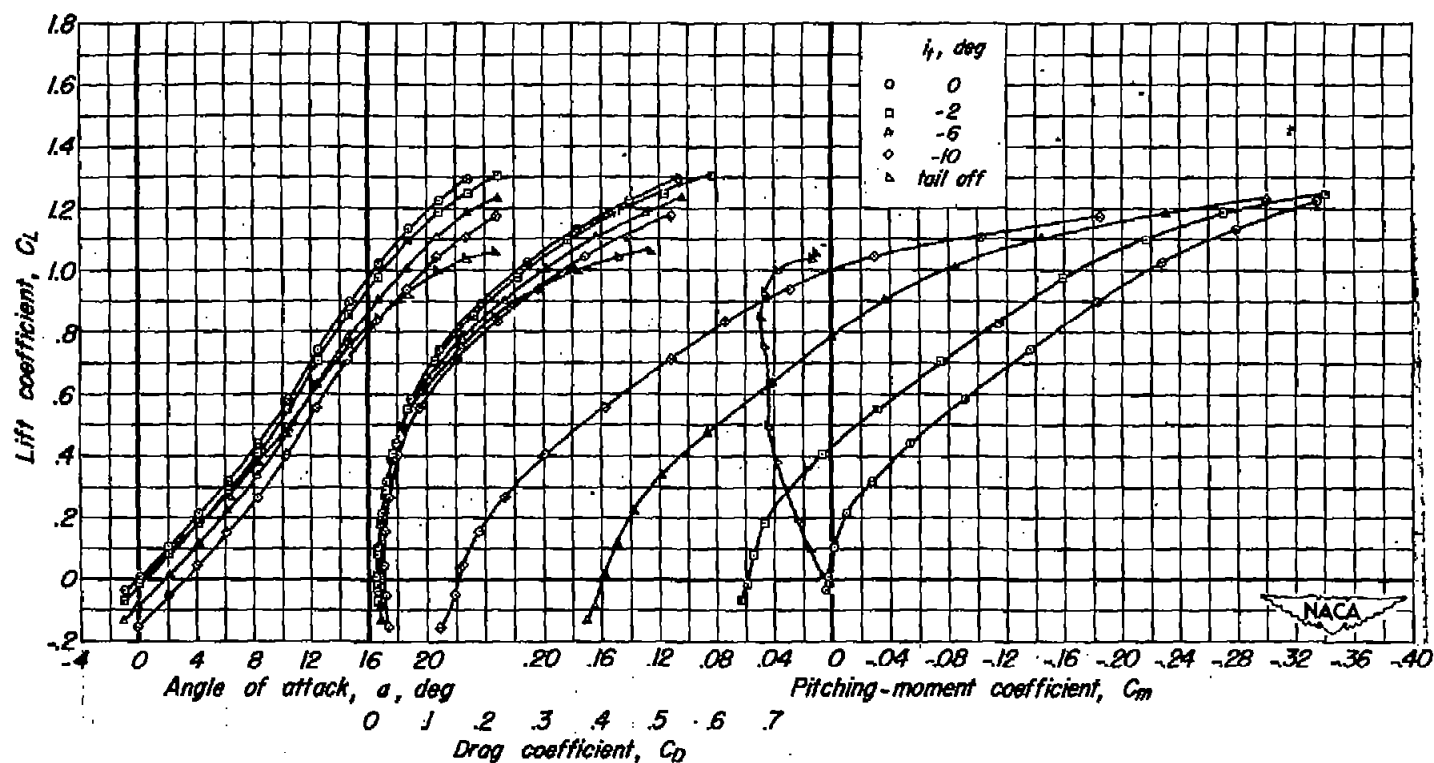
(a) C_L vs α , C_D , C_m

Figure 7.— Characteristics of the wing-fuselage vertical-tail configurations with two different trailing-edge flap deflections. c.g., $0.25\bar{c}$.



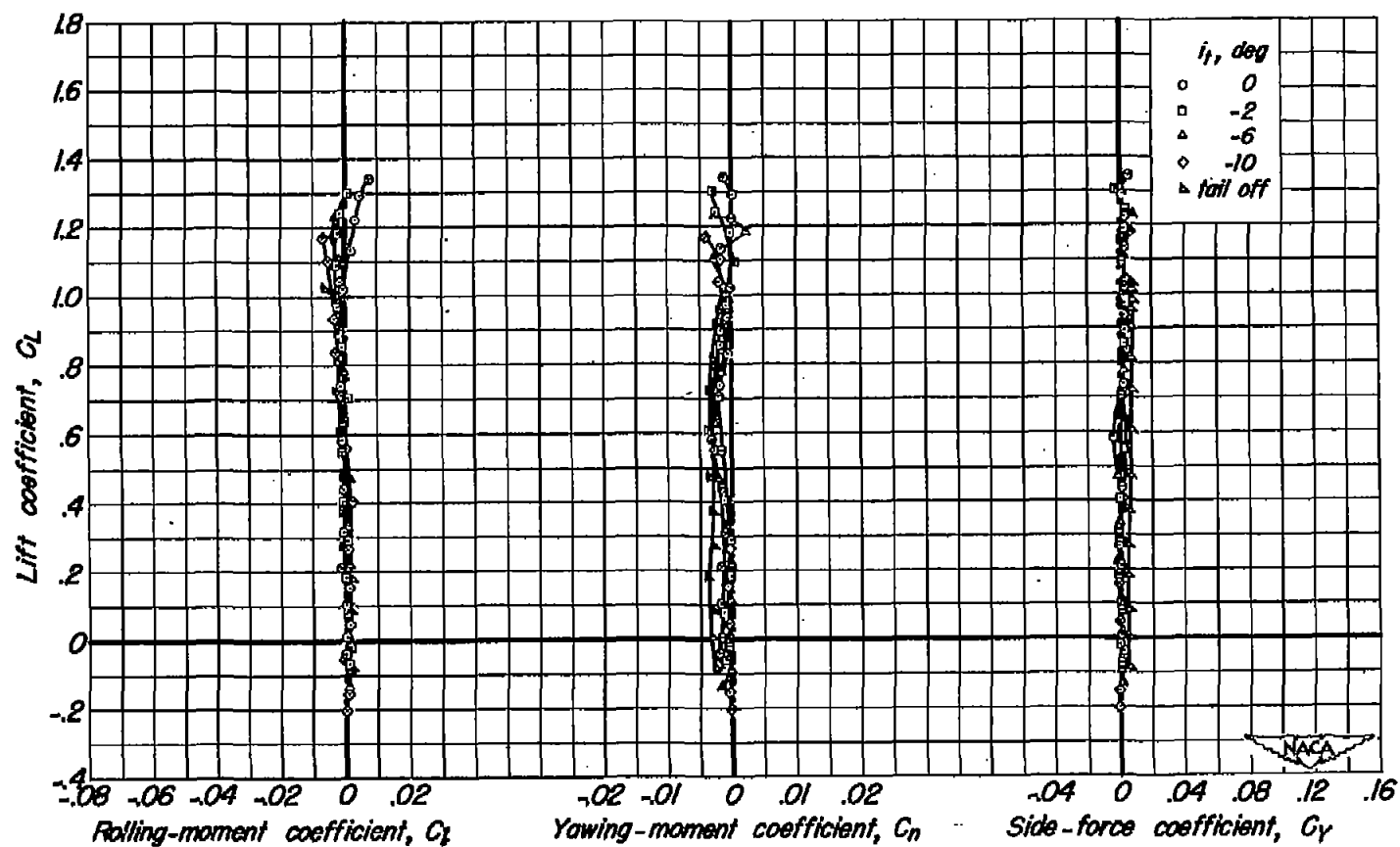
(b) C_L vs C_l , C_n , C_y

Figure 7.— Concluded.



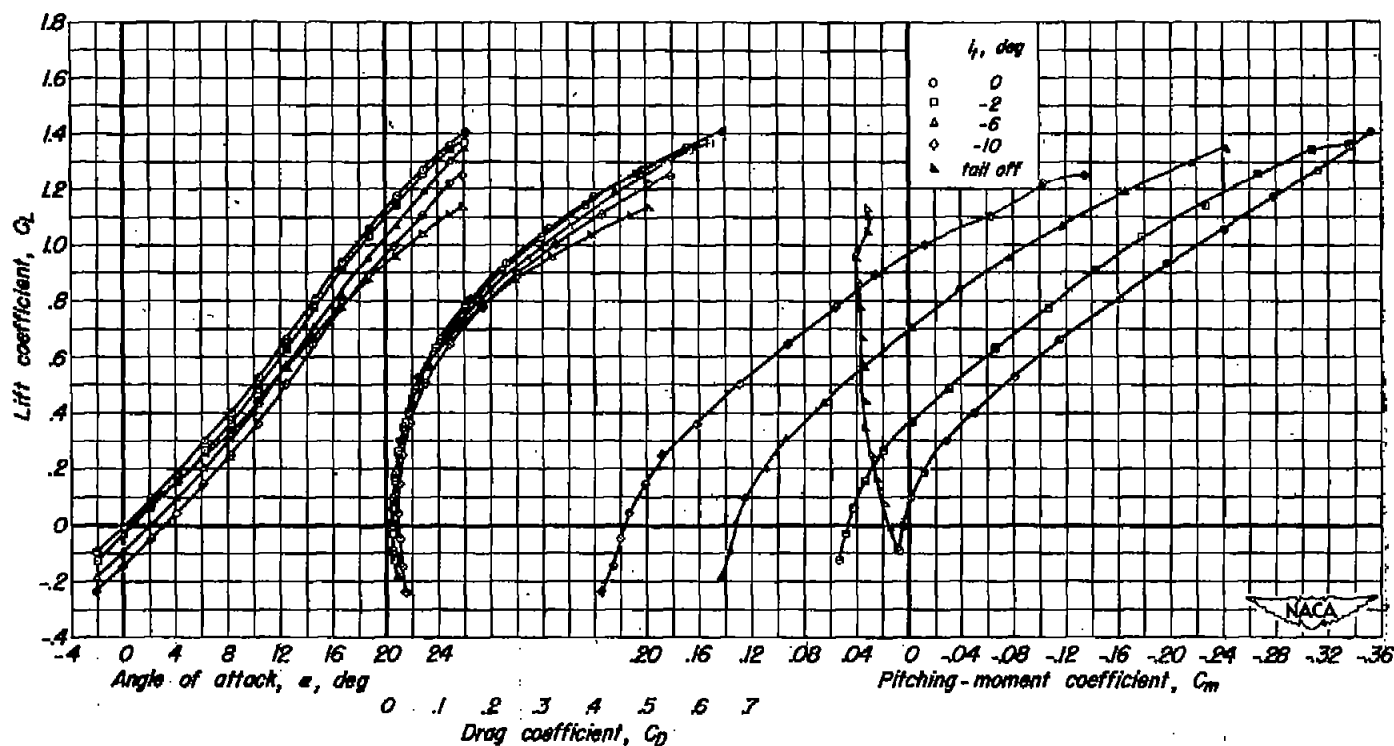
(a) C_L vs α , C_D , C_m

Figure 8.— Characteristics of the model having the wing of taper ratio 0.33 with the horizontal tail in the low position. δ_f , 0° ; $\frac{z}{b/2}$, 0; c.g., 0.338 \bar{c} .



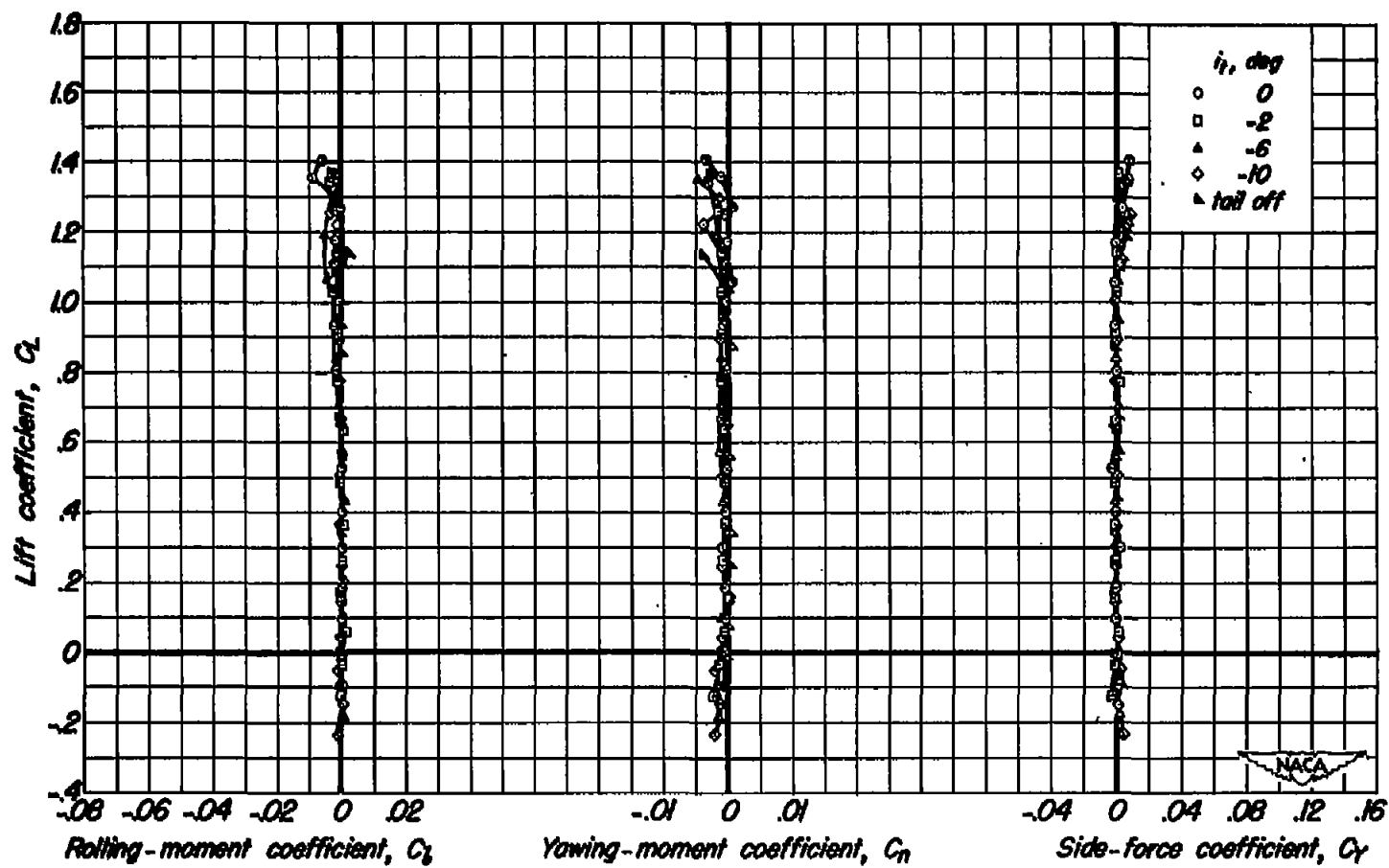
(b) C_L vs C_l , C_n , C_y

Figure 8.— Concluded.



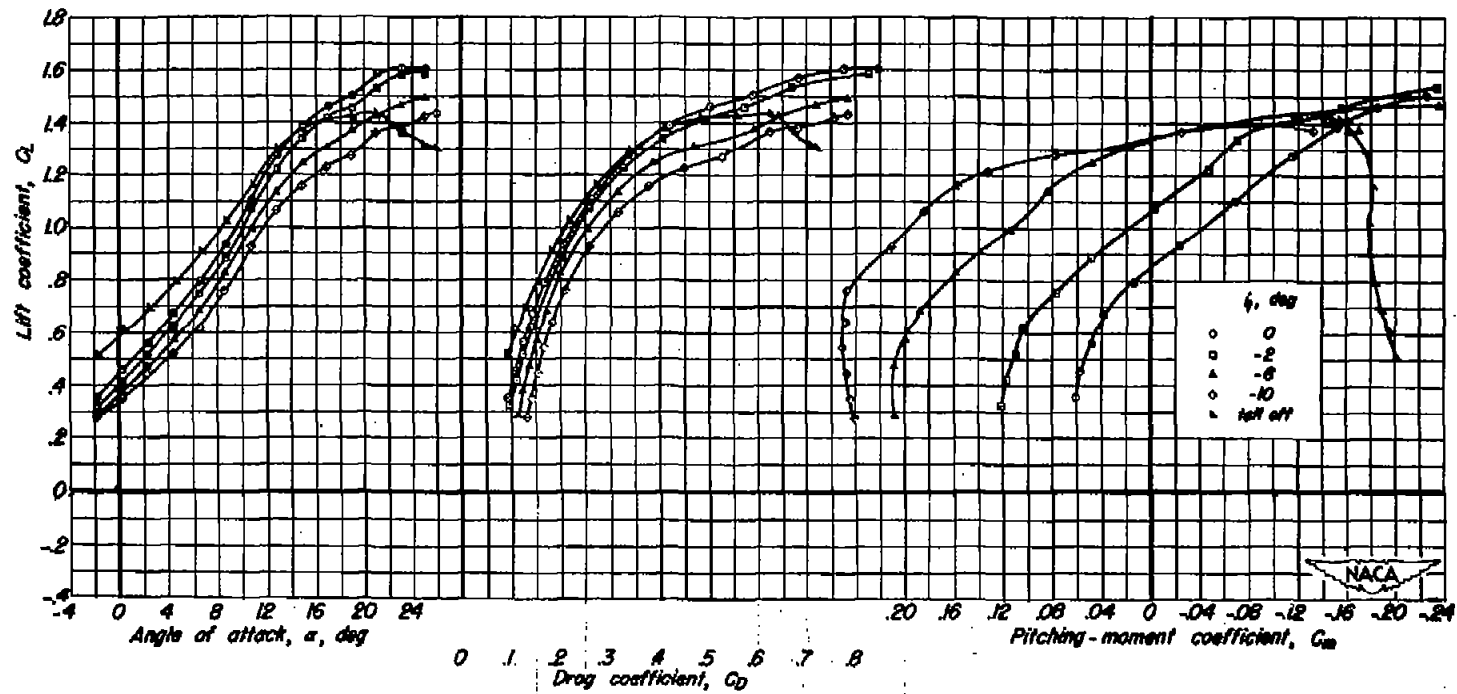
(a) C_L vs α , C_D , C_m

Figure 9.— Characteristics of the model having the wing of taper ratio 0.20 with the horizontal tail in the low position. $\delta_f, 0^\circ$; $\frac{z}{b/2}, 0$; c.g., 0.369c.



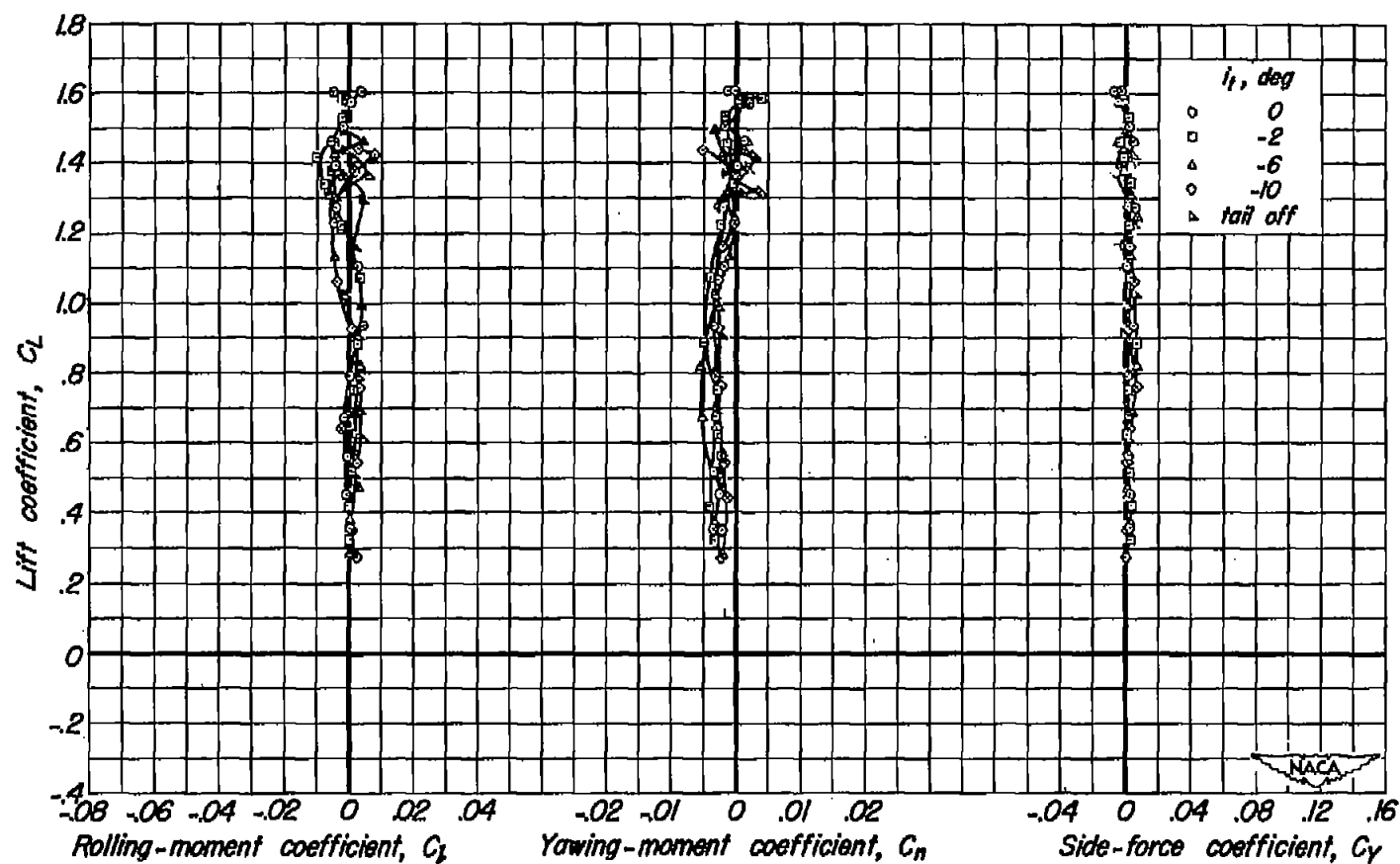
(b) C_L vs C_L , C_n , C_Y

Figure 9.- Concluded.



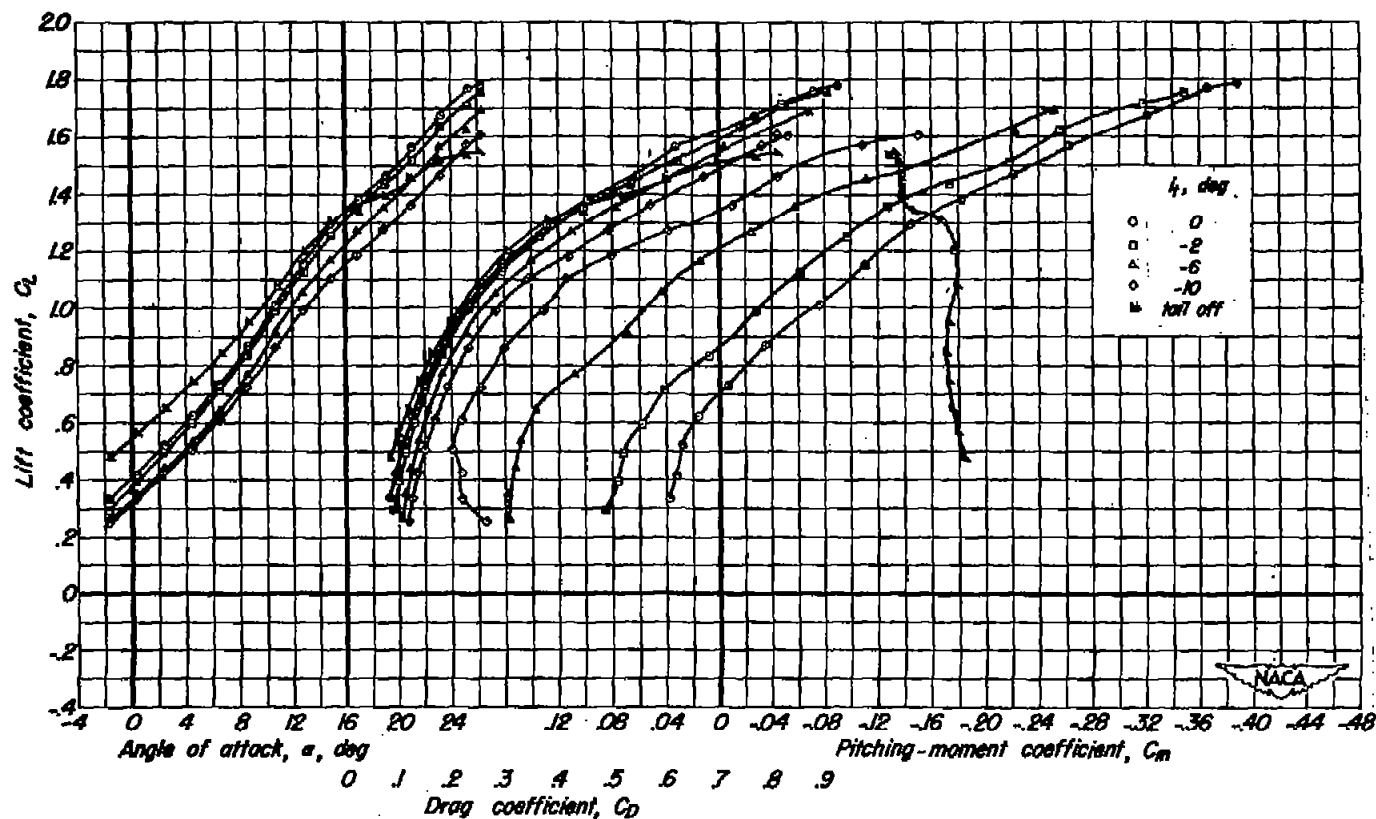
(a) C_L vs α , C_D , C_m

Figure 10.— Characteristics of the model having the wing of taper ratio 0.33 with the horizontal tail in the low position. δ_f , 40° ; $\frac{z}{b/2}$, 0; c.g., 0.338c.



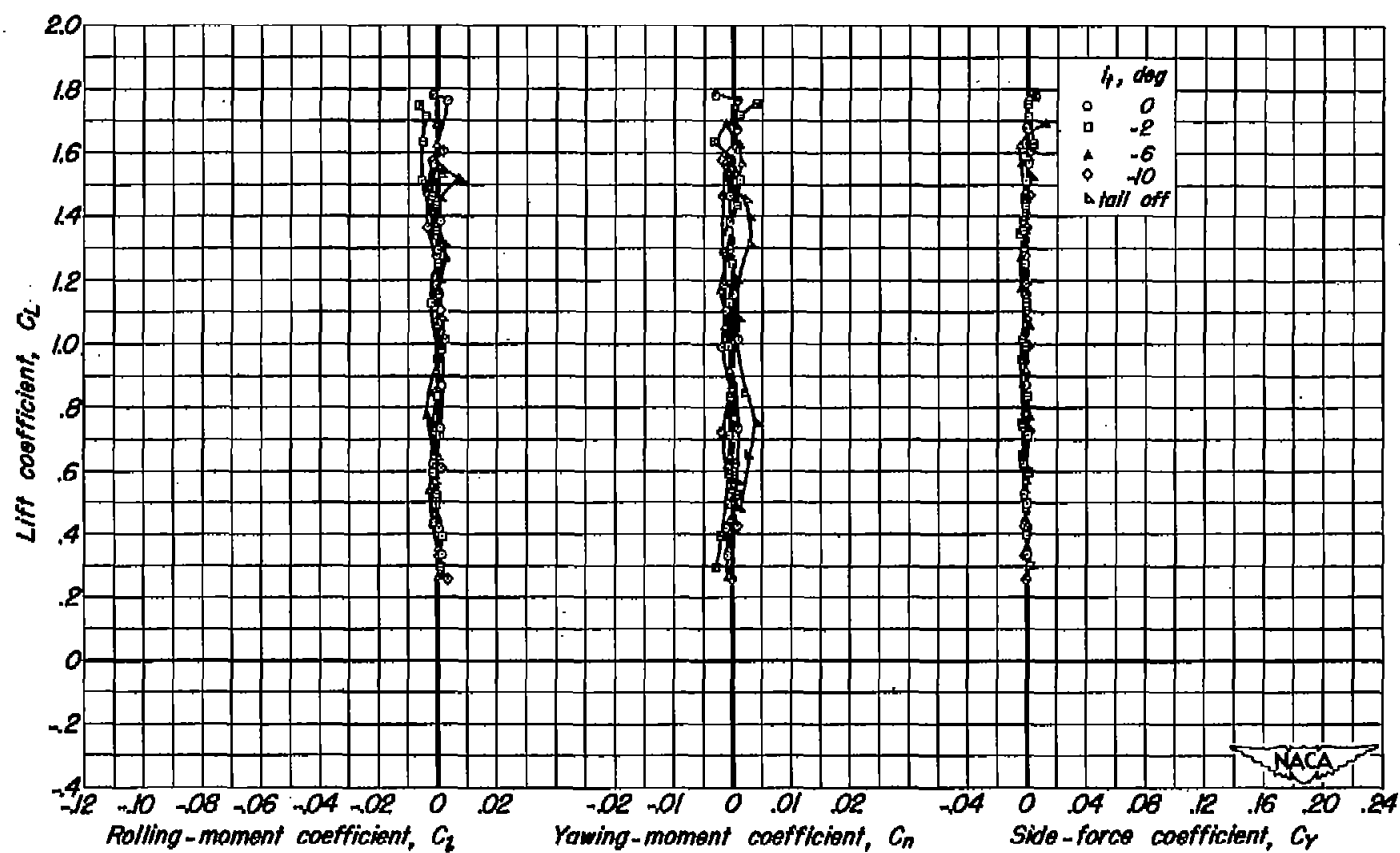
(b) C_L vs C_l , C_n , C_y

Figure 10.- Concluded.



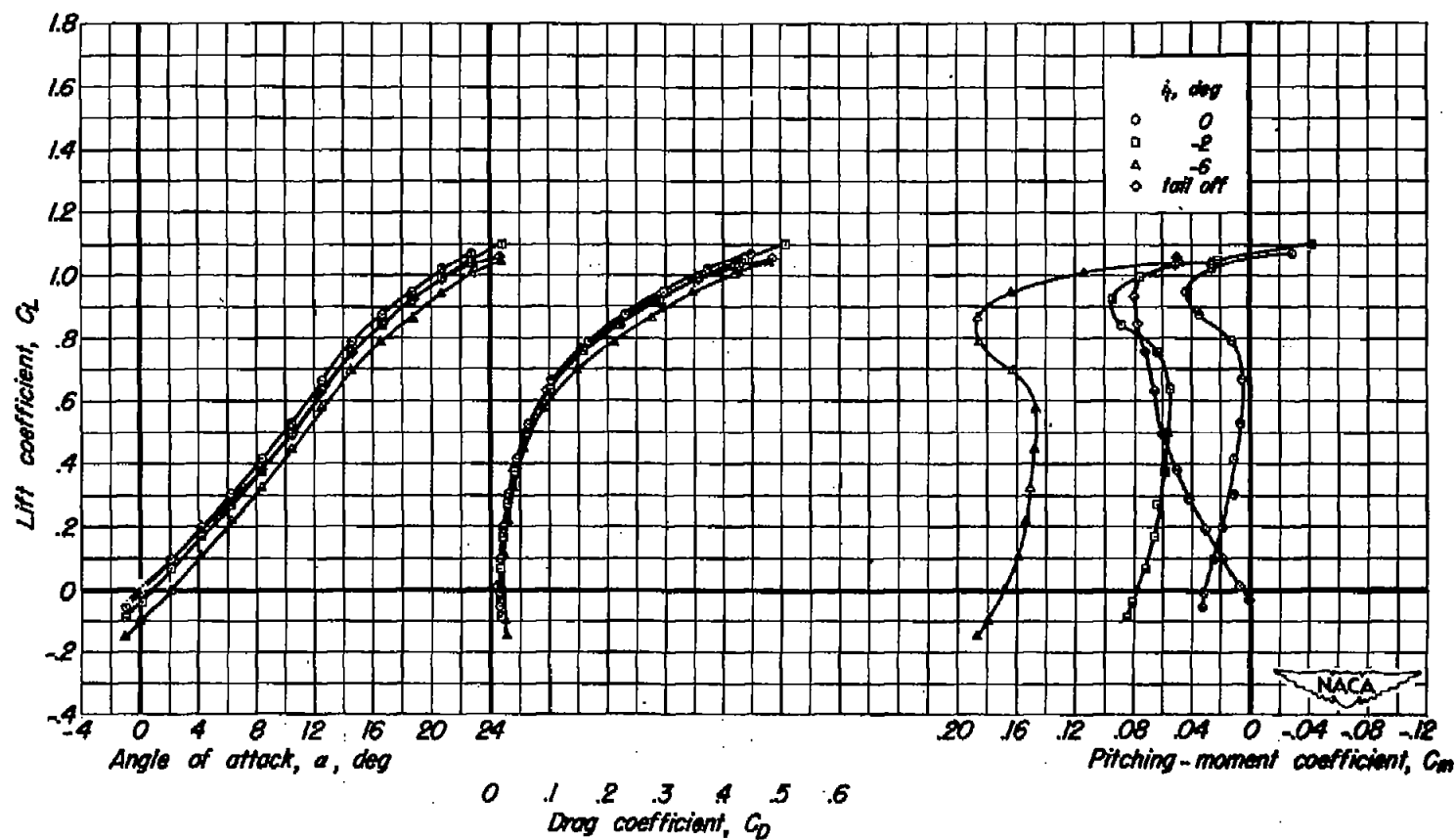
(a) C_L vs α , C_D , C_m

Figure 11.— Characteristics of the model having the wing of taper ratio 0.20 with the horizontal tail in the low position. δ_f , 40° ; $\frac{I}{b^2}$, 0; c.g., $0.369\bar{c}$.



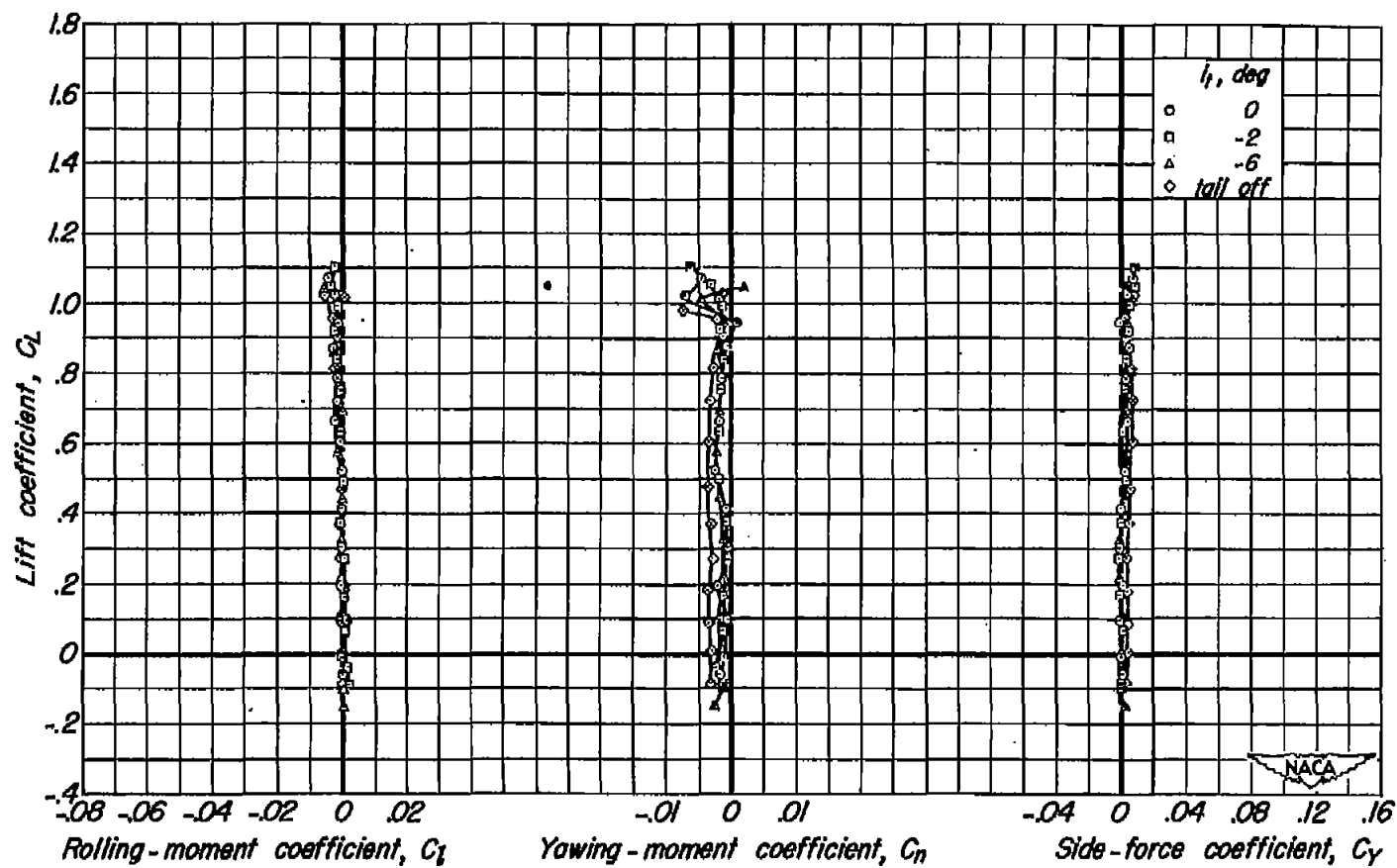
(b) C_L vs C_l , C_n , C_y

Figure 11.- Concluded.



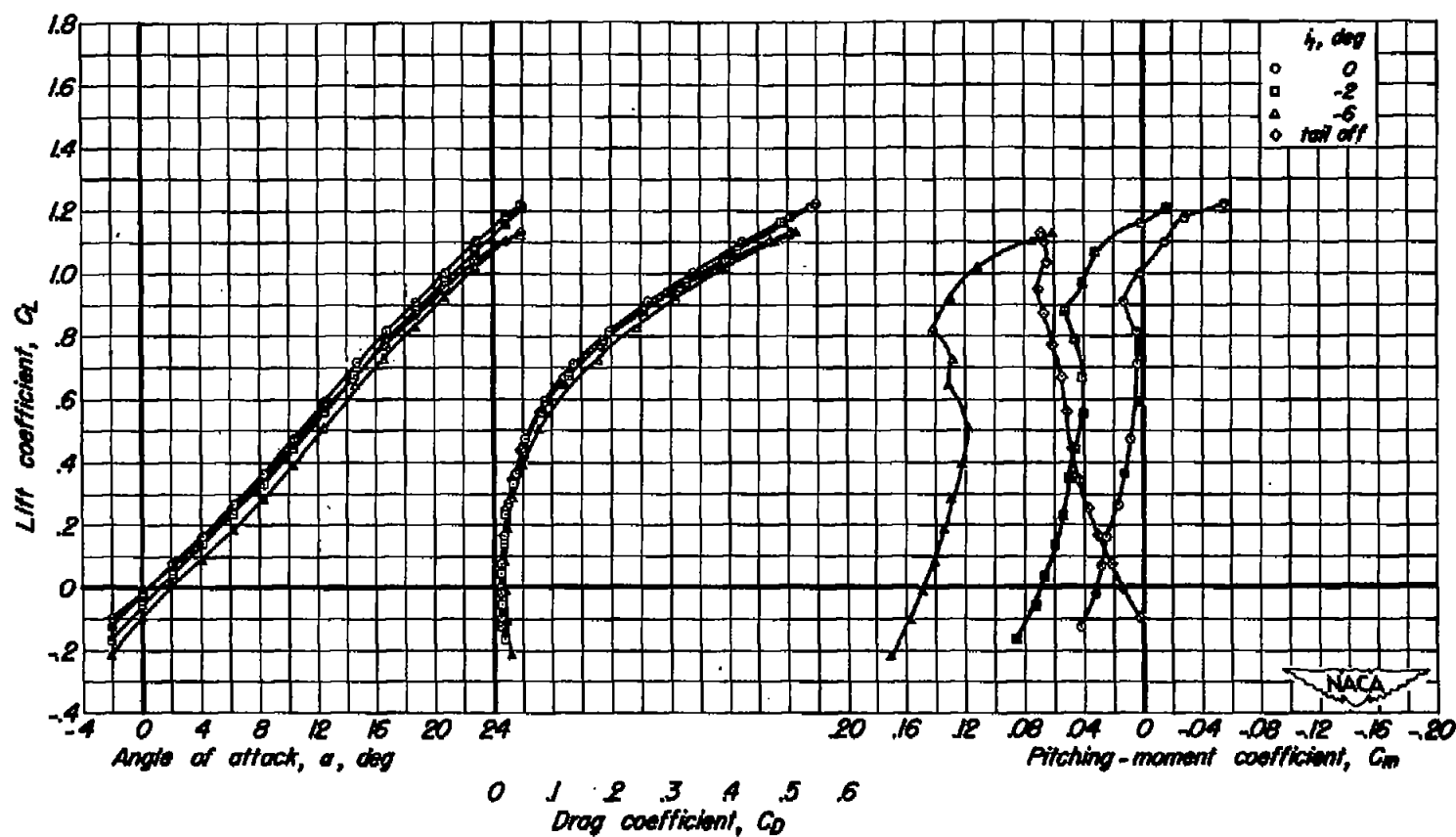
(a) C_L vs α , C_D , C_m

Figure 12.— Characteristics of the model having the wing of taper ratio 0.33 with the horizontal tail in the middle position. $\delta_f, 0^\circ$; $\frac{z}{b/2}, 0.269$; c.g., 0.372c.



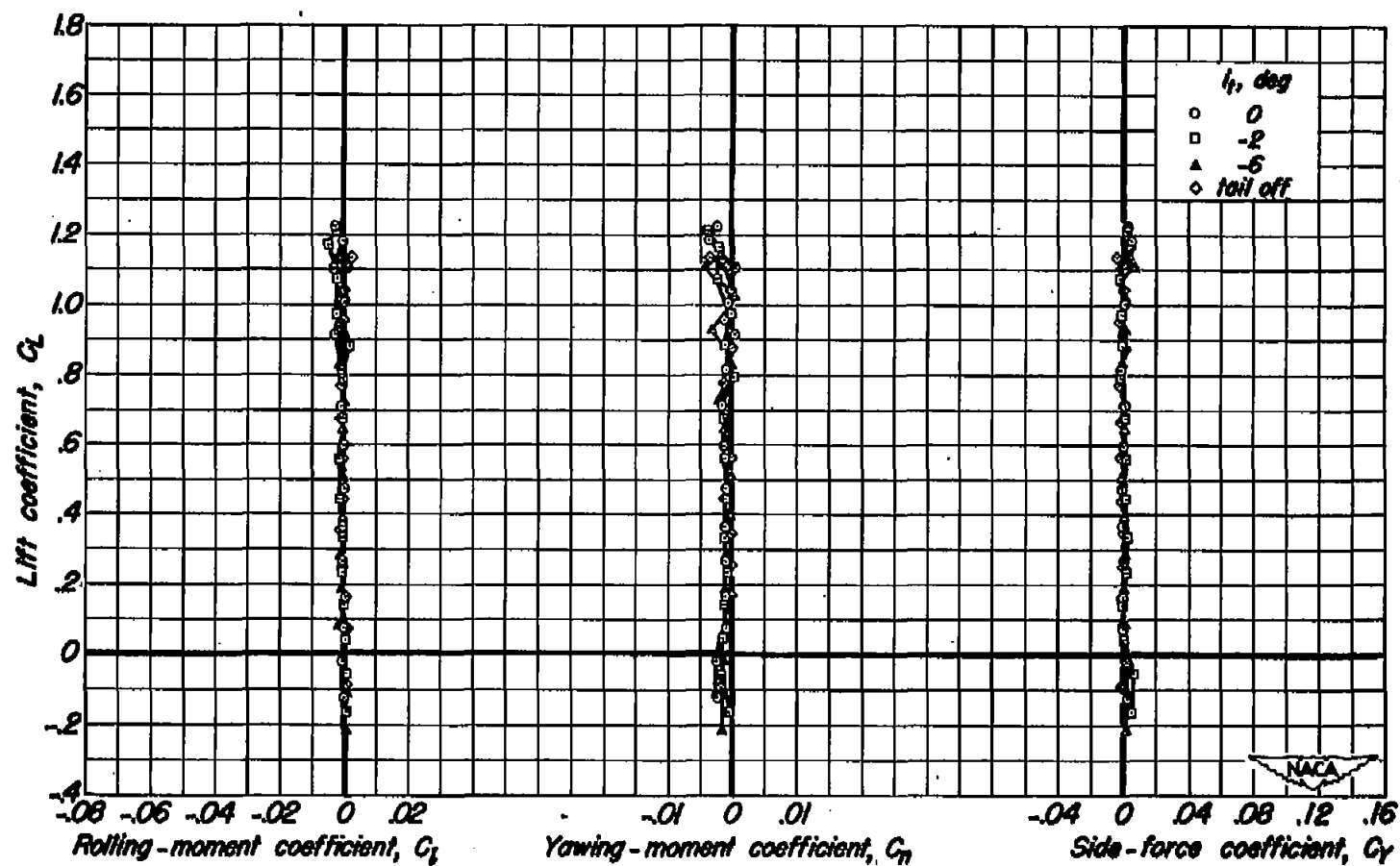
(b) C_L vs C_l, C_n, C_Y

Figure 12.- Concluded.



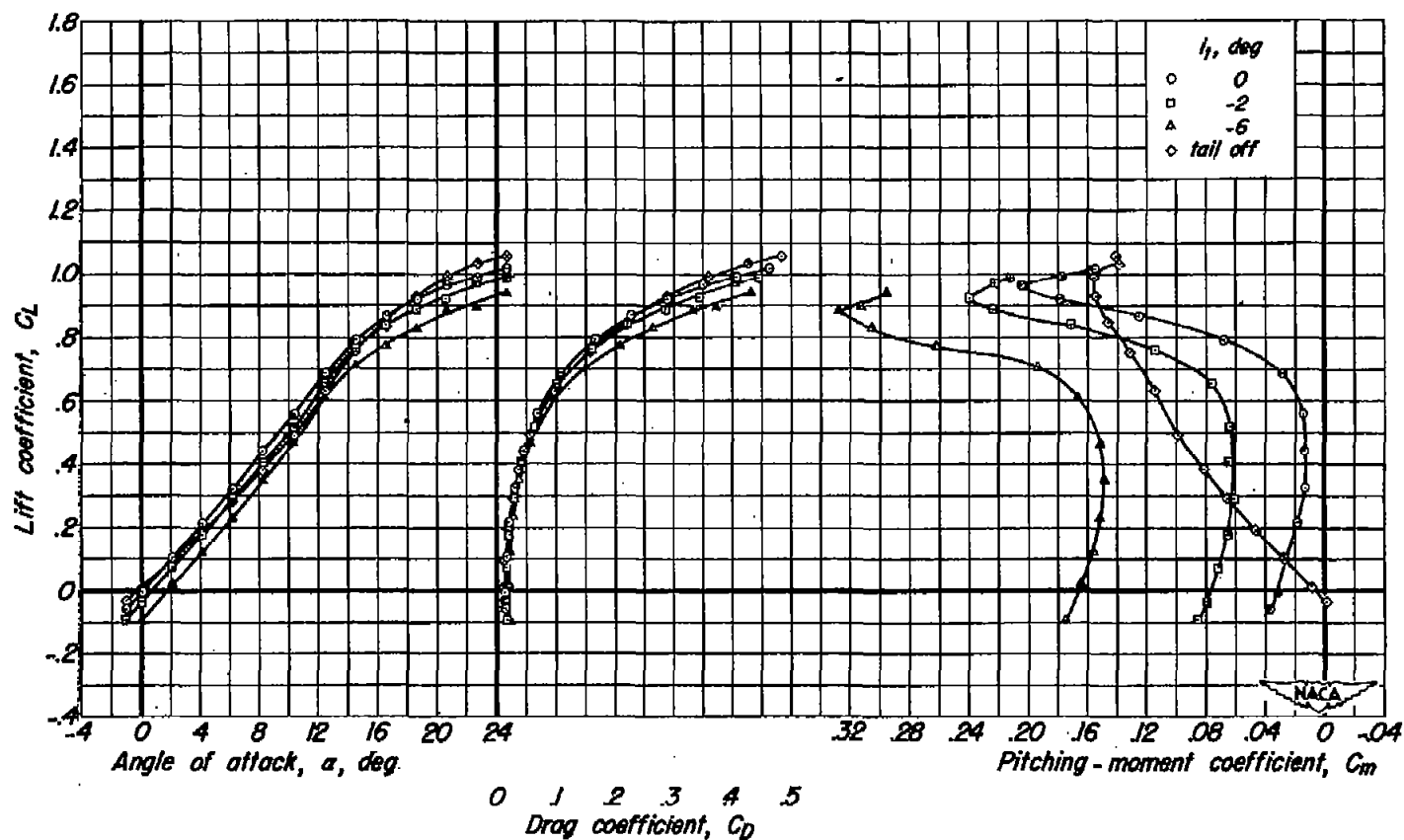
(a) C_L vs α , C_D , C_m

Figure 13.— Characteristics of the model having the wing of taper ratio 0.20 with the horizontal tail in the middle position. δ_f , 0° ; $\frac{z}{b/2}$, 0.259; c.g., 0.400c.



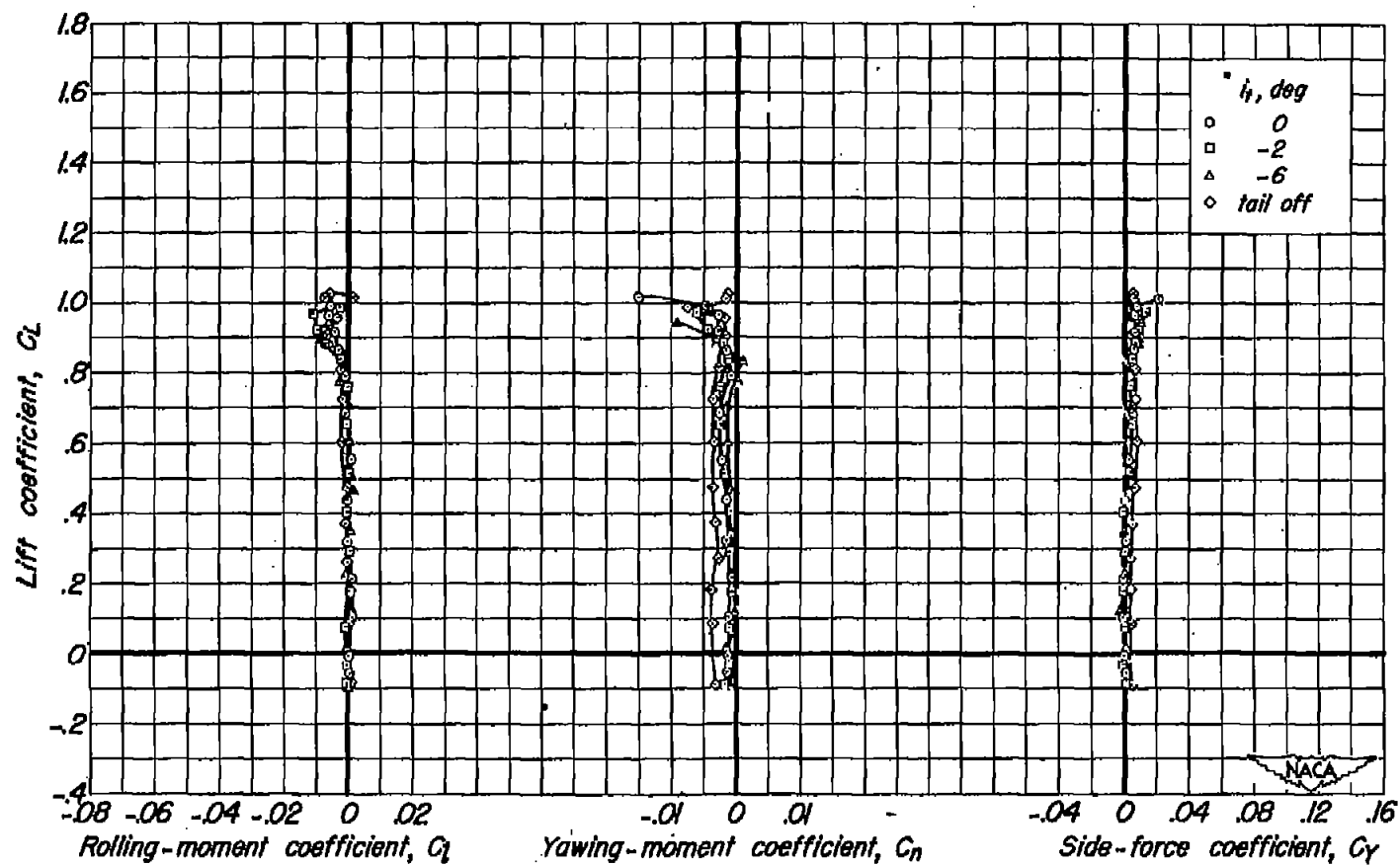
(b) C_L vs C_l , C_n , C_Y

Figure 13.- Concluded.



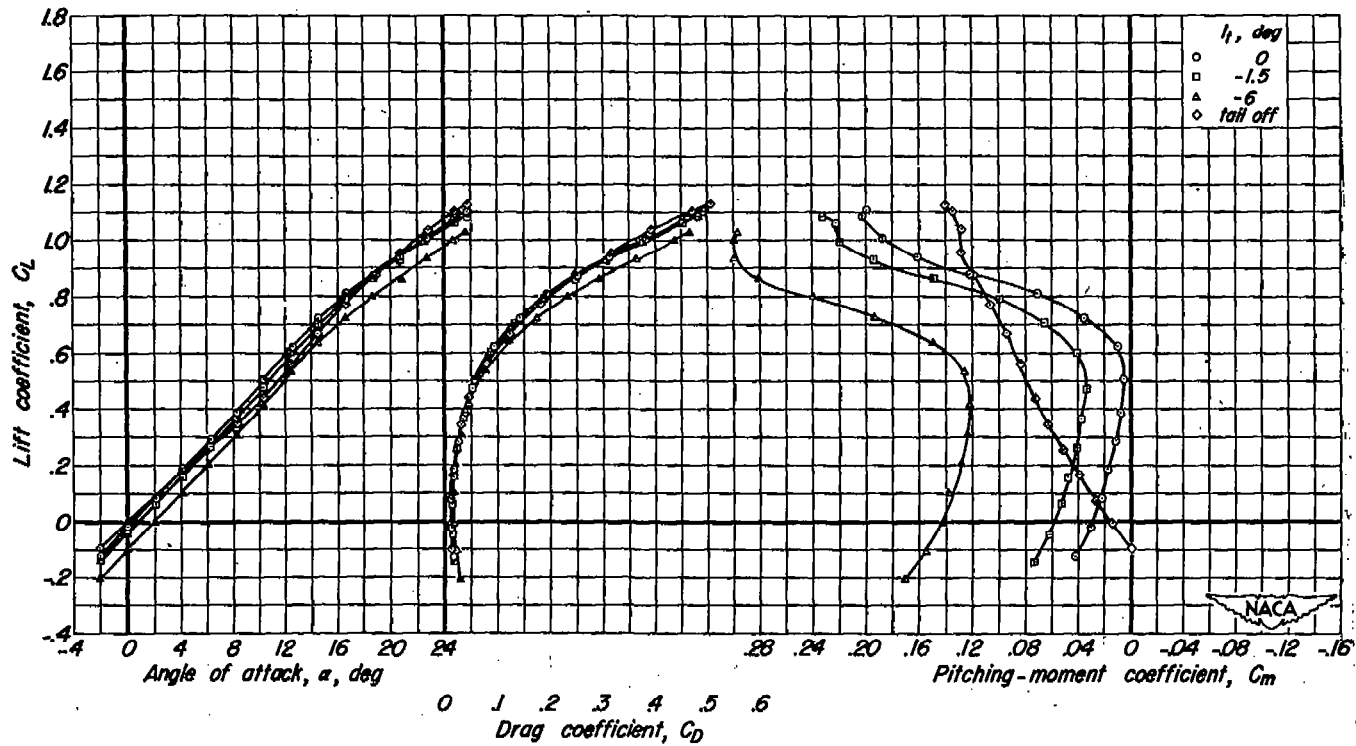
(a) C_L vs α , C_D , C_m

Figure 14.— Characteristics of the model having the wing of taper ratio 0.33 with the horizontal tail in the high position. δ_f , 0° ; $\frac{z}{b/2}$, 0.537; c.g., 0.451*l*.



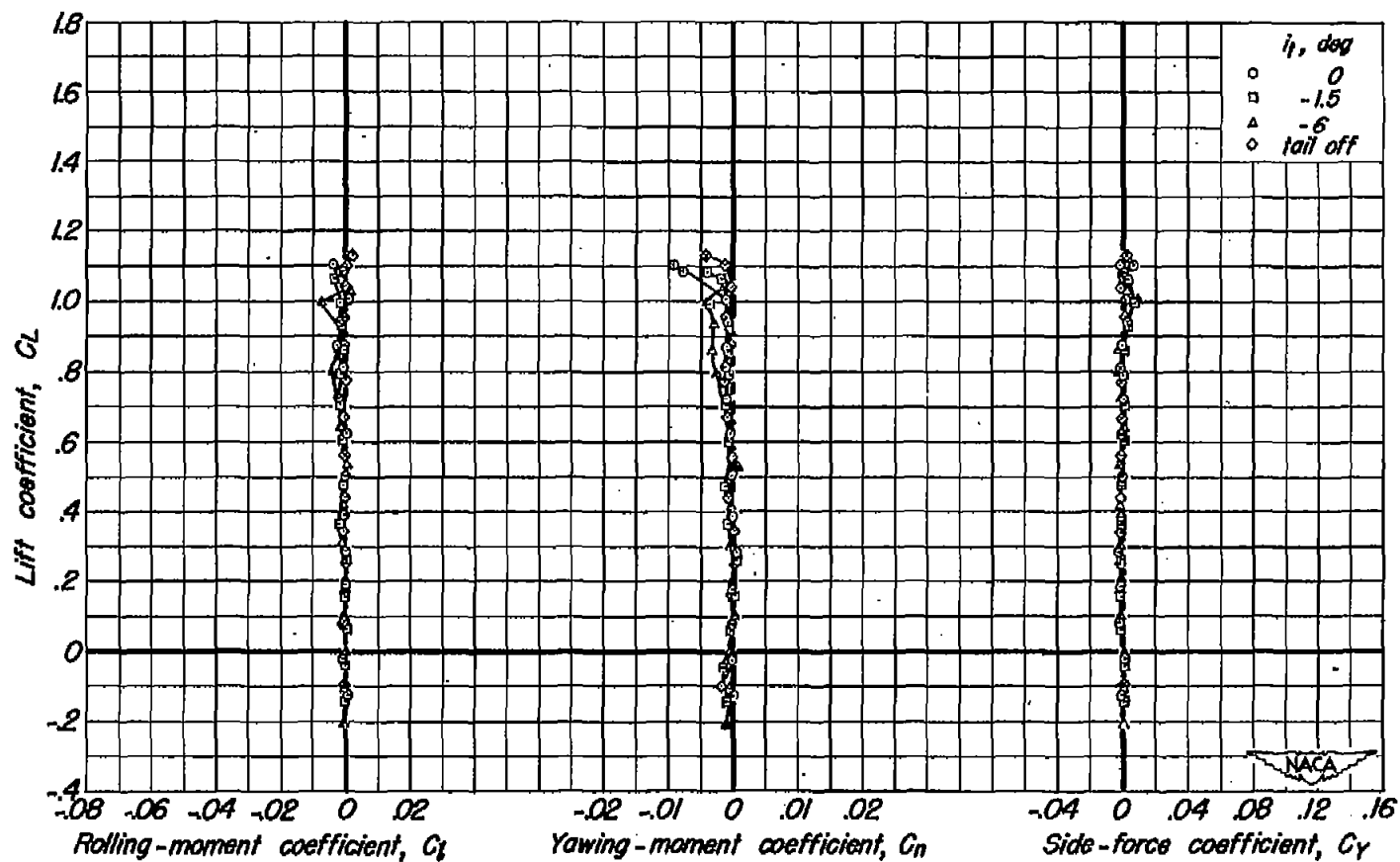
(b) C_L vs C_l , C_n , C_y

Figure 14.- Concluded.



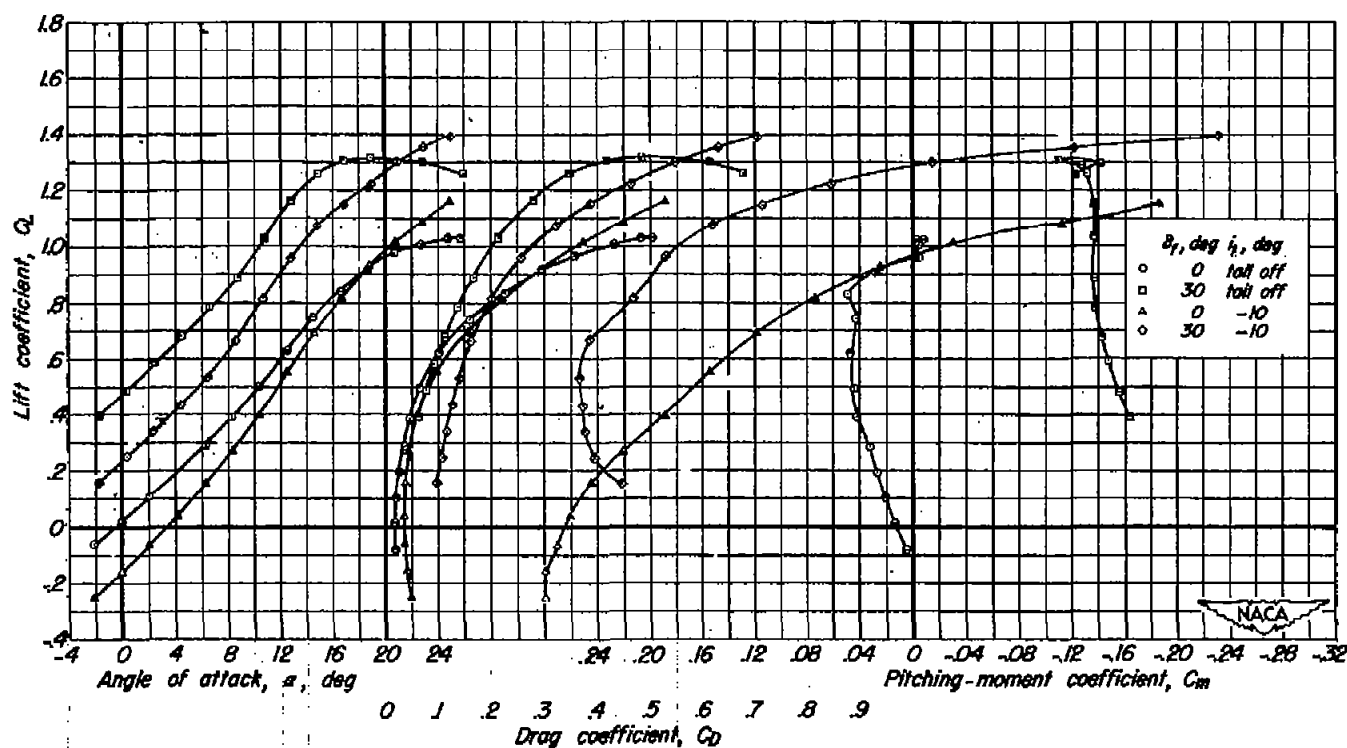
(a) C_L vs α , C_D , C_m

Figure 15.— Characteristics of the model having the wing of taper ratio 0.20 with the horizontal tail in the high position. δ_f , 0° ; $\frac{z}{b/2}$, 0.516; c.g., 0.457 \bar{c} .



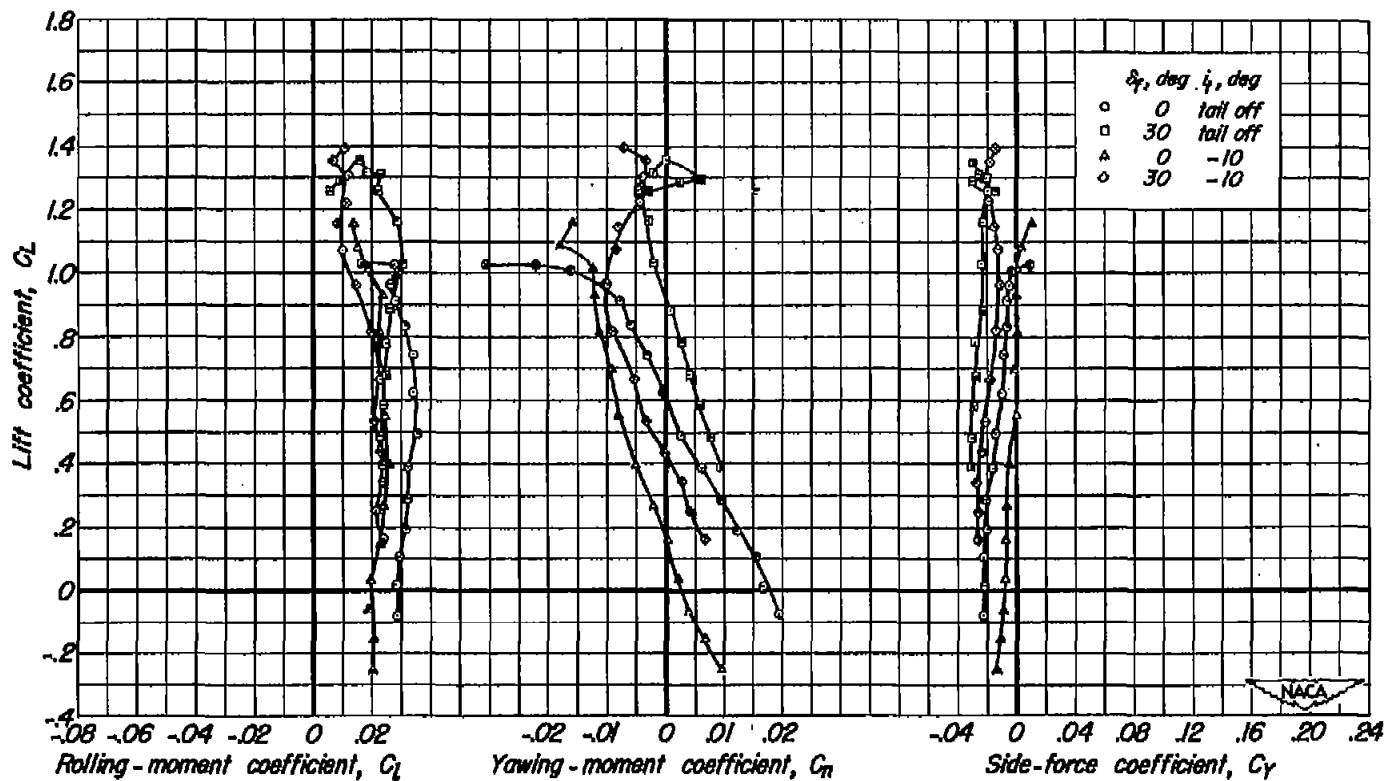
(b) C_L vs C_l , C_n , C_y

Figure 15.— Concluded.



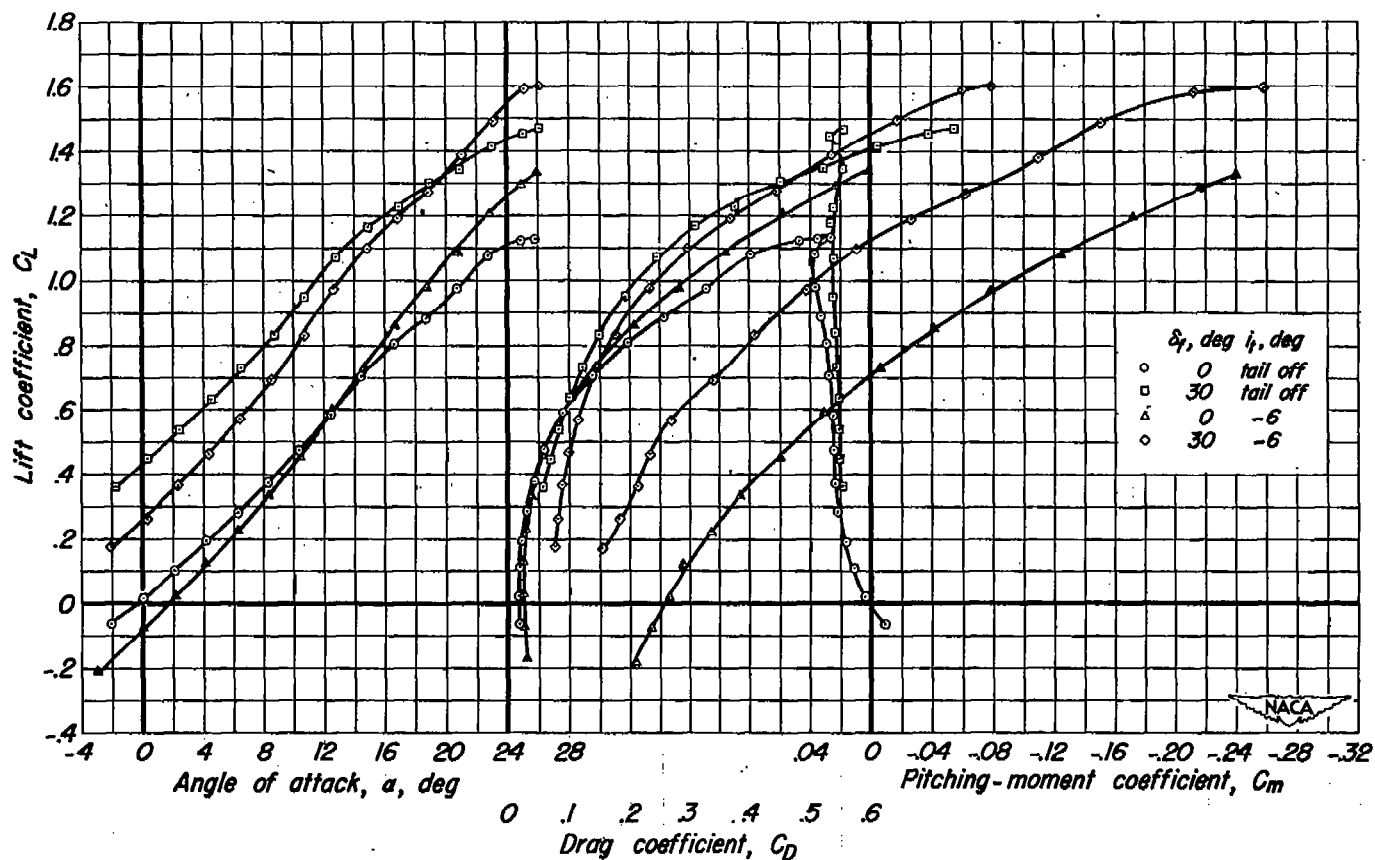
(a) C_L vs α , C_D , C_m

Figure 16.— Characteristics of the model having the wing of taper ratio 0.33 with the flaps used as lateral controls. $\frac{z}{b/2}$, 0; c.g., 0.338 \bar{c} ; δ_{lf} , 20°.



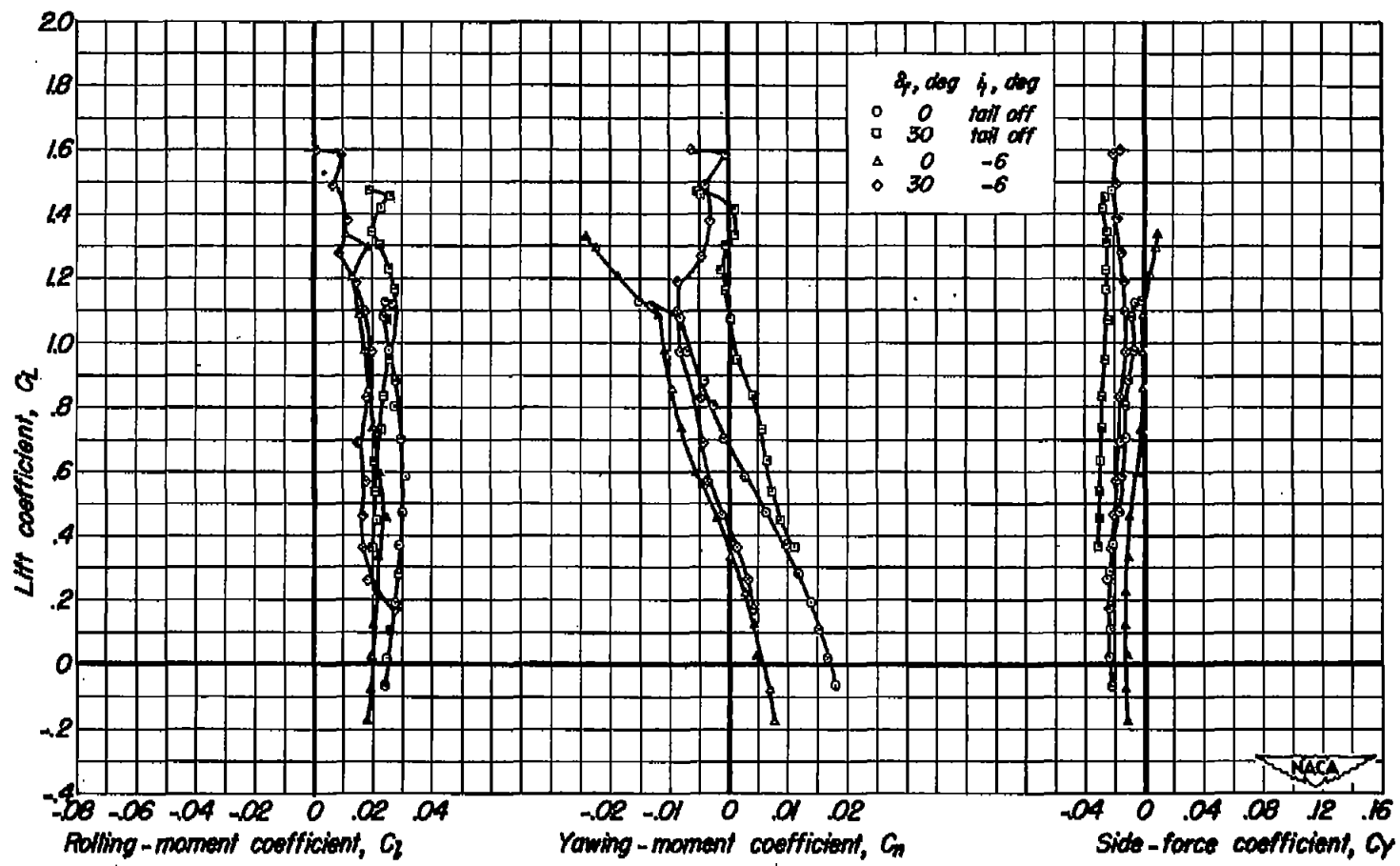
(b) C_L vs C_l , C_n , C_y

Figure 16.— Concluded.



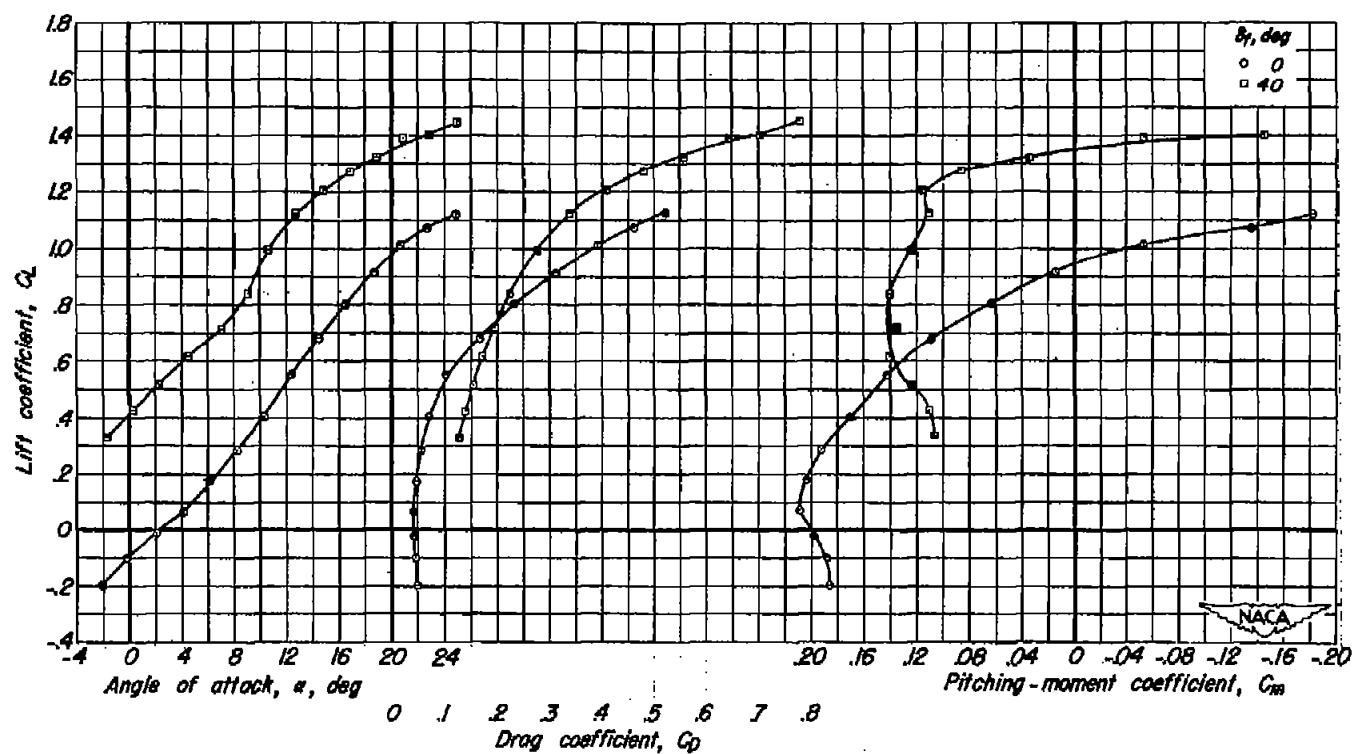
(a) C_L vs α , C_D , C_m

Figure 17.— Characteristics of the model having the wing of taper ratio 0.20 with the flaps used as lateral controls. $\frac{z}{b/2}$, 0; c.g., 0.369 \bar{c} ; δ_{lf} , 20°.



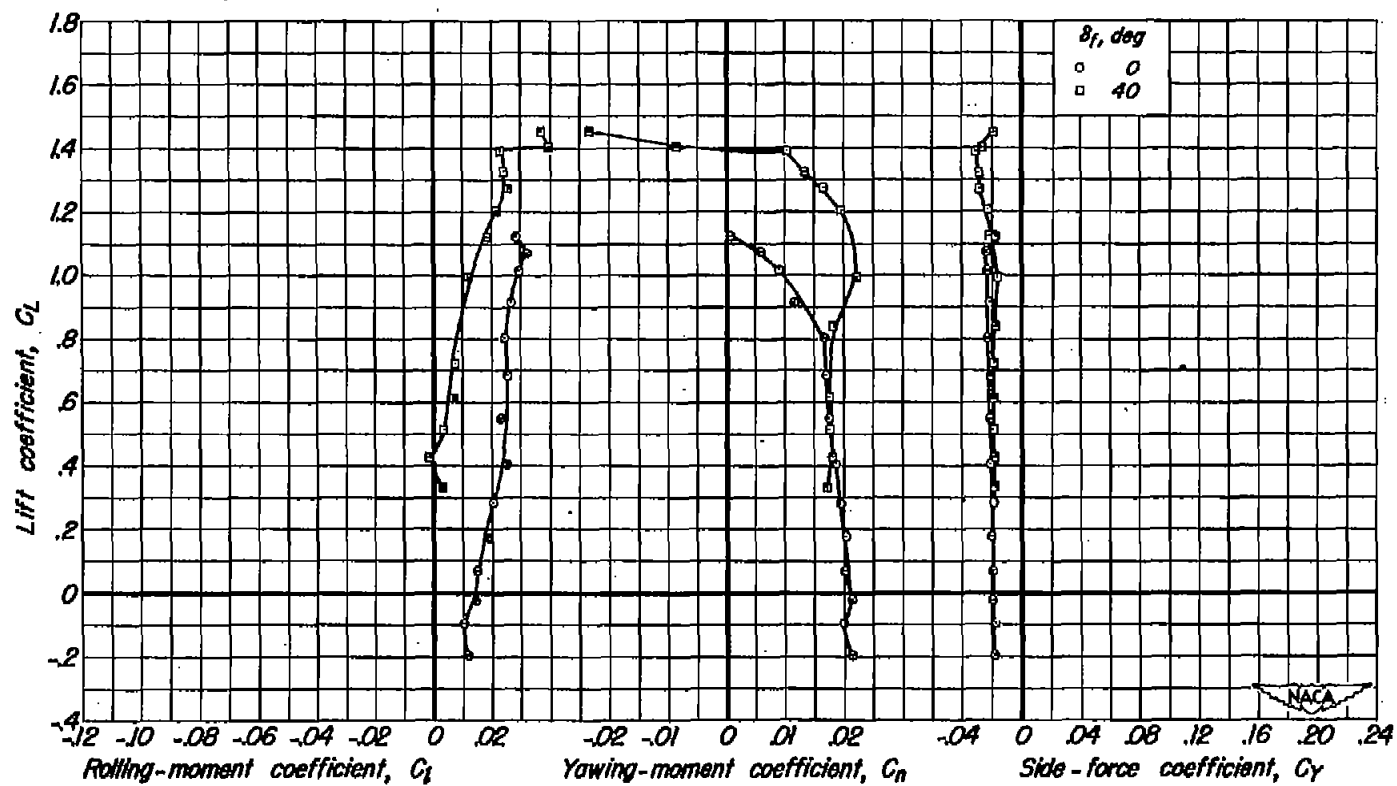
(b) C_L vs C_l , C_n , C_y

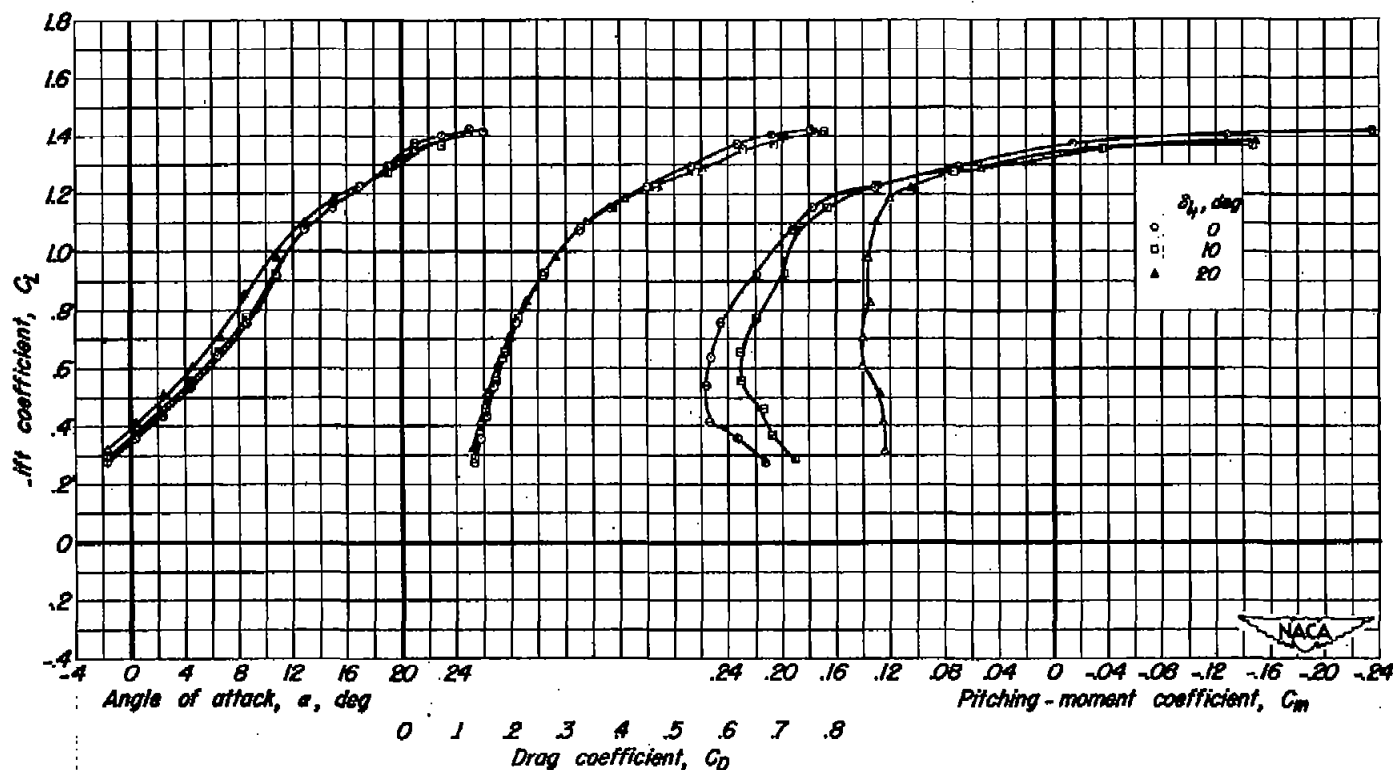
Figure 17.- Concluded.



(a) C_L vs α , C_D , C_m

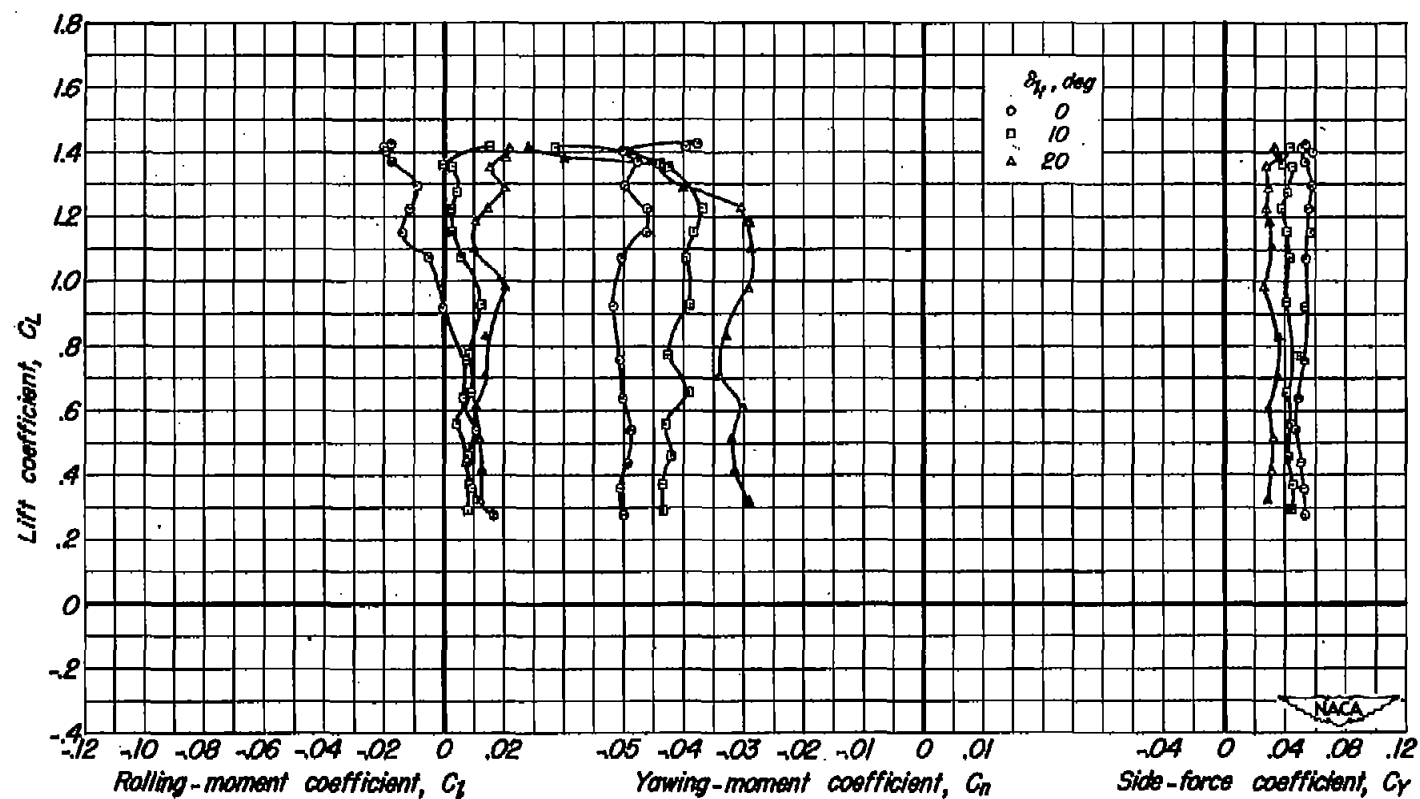
Figure 18.— Characteristics of the model having the wing of taper ratio 0.33 with the horizontal tail used as a lateral control. $\frac{z}{b/2}$, 0; c.g., 0.338 \bar{c} ; δ_{f1} , 20°; i_f , -10°.





(a) C_L vs α , C_D , C_m

Figure 19.— Characteristics of the model having the wing of taper ratio 0.33 with the horizontal tail used as a lateral control, and the rudder deflected 10° . $\frac{z}{b/2}$, 0; δ_f , 40° ; c.g., 0.338 \bar{c} ; δ_r , 10° ; i_f , -10° .



(b) C_L vs C_L , C_n , C_y

Figure 19.— Concluded.

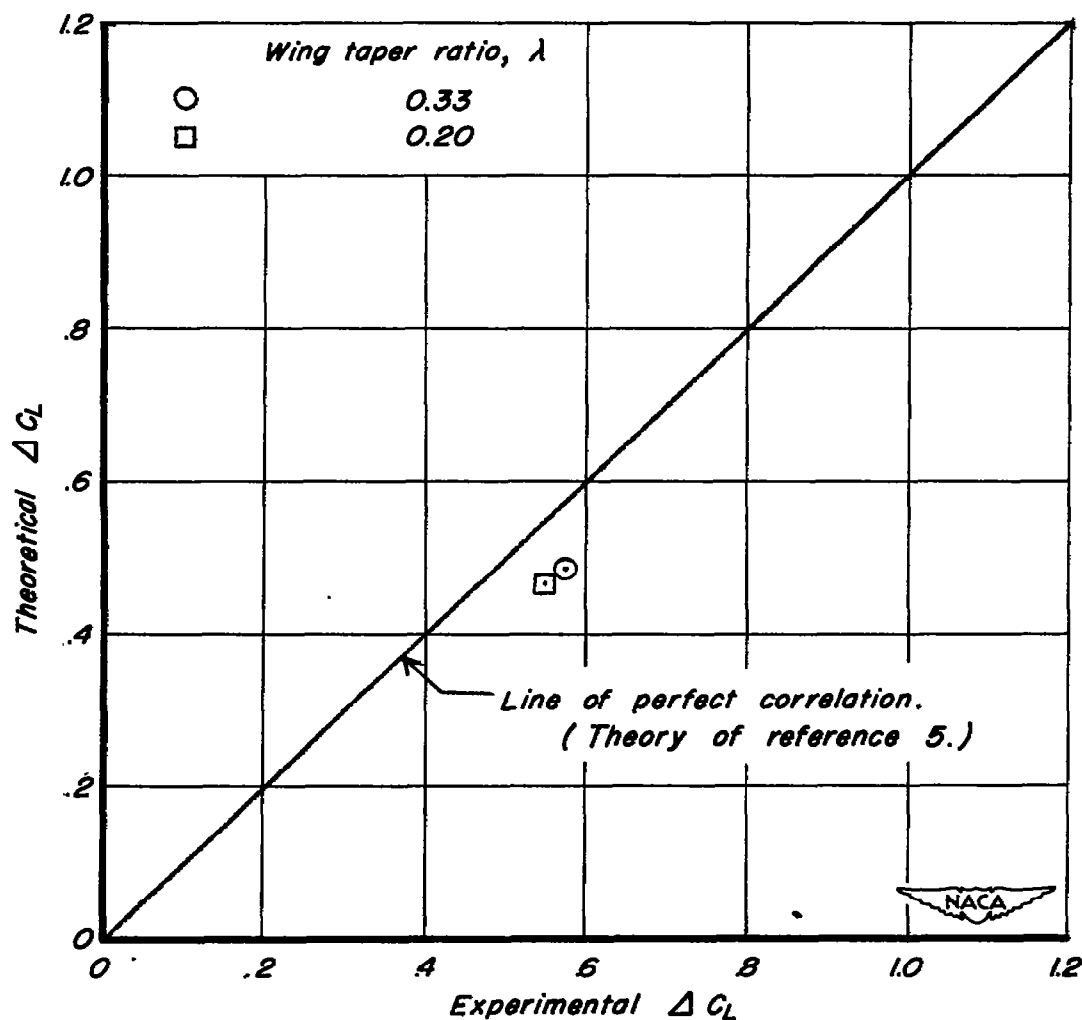


Figure 20.— Experimental and theoretical increments of lift coefficient with flaps deflected to 40° for two wing-fuselage vertical-tail configurations. $\alpha, 0^\circ$; $\delta_r, 0^\circ$.

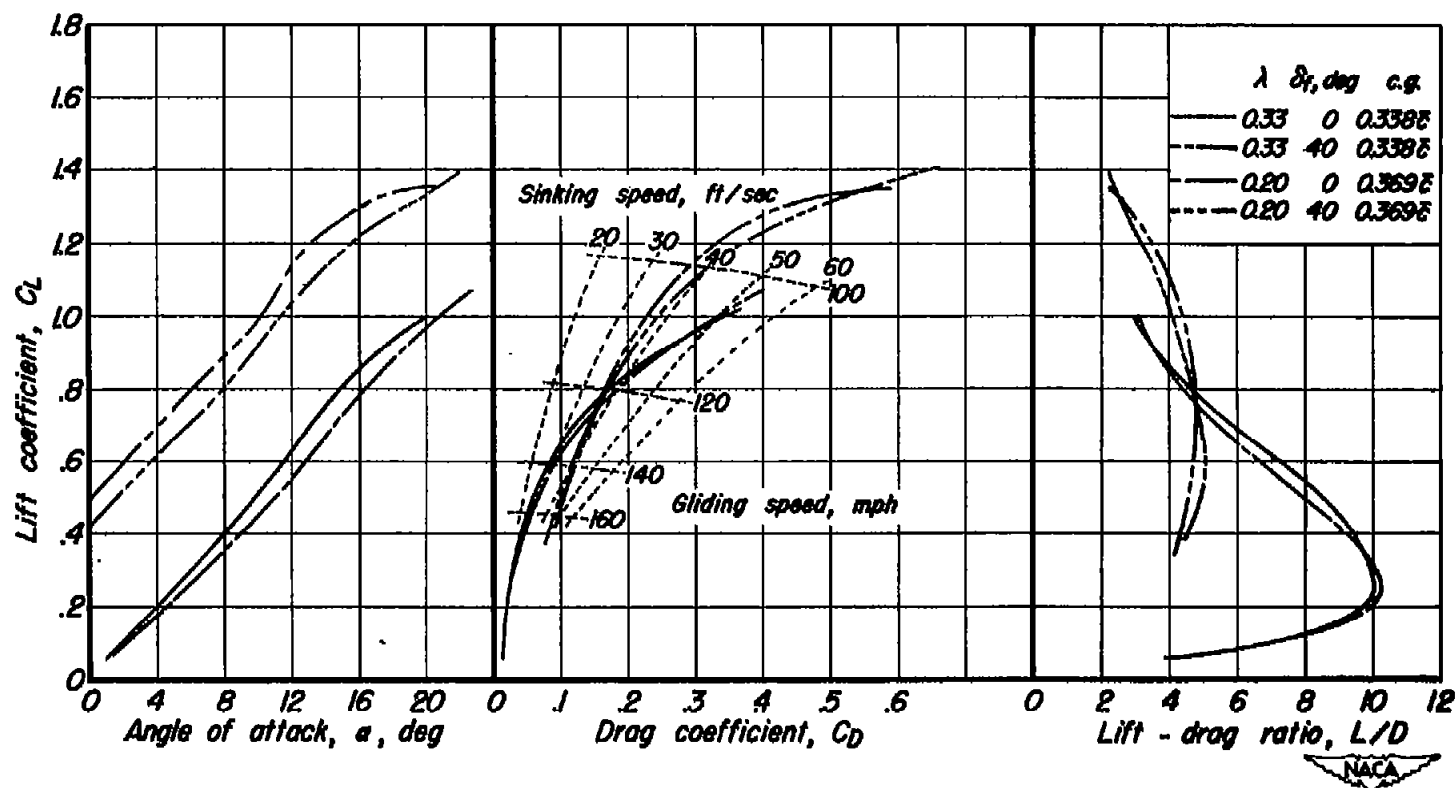


Figure 21.— Comparison of the lift and drag characteristics of trimmed, aspect ratio 2 trapezoidal-wing airplanes having all-movable horizontal tails. $\frac{z}{b/2}$, 0; W/S , 30 pounds per square foot.

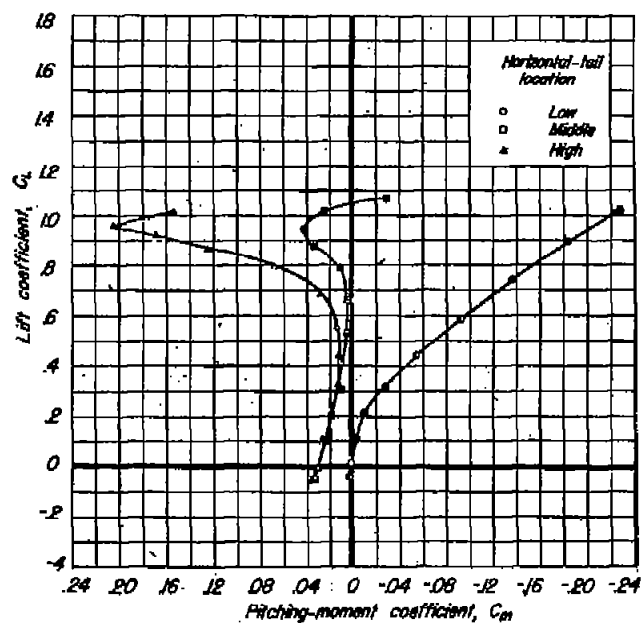
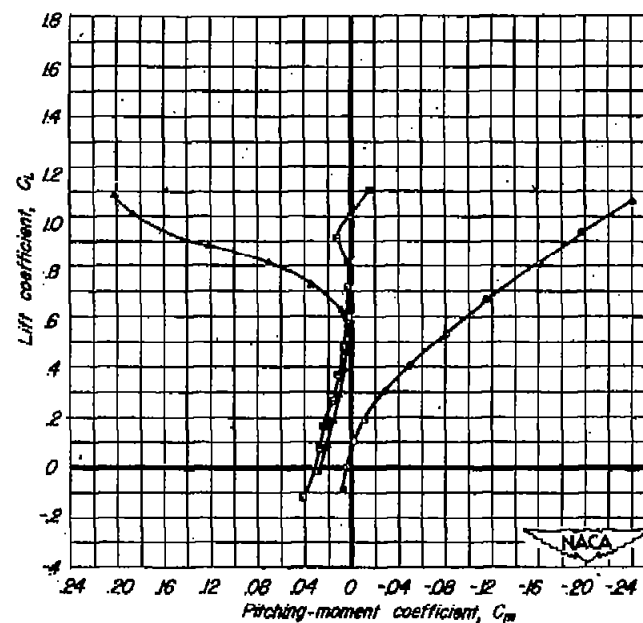
(a) $\lambda, 0.33$ (b) $\lambda, 0.20$

Figure 22.— Summary of the effect of the vertical location of the horizontal tail on the pitching-moment coefficient of both models. $i_f, 0^\circ$; $\delta_f, 0^\circ$.

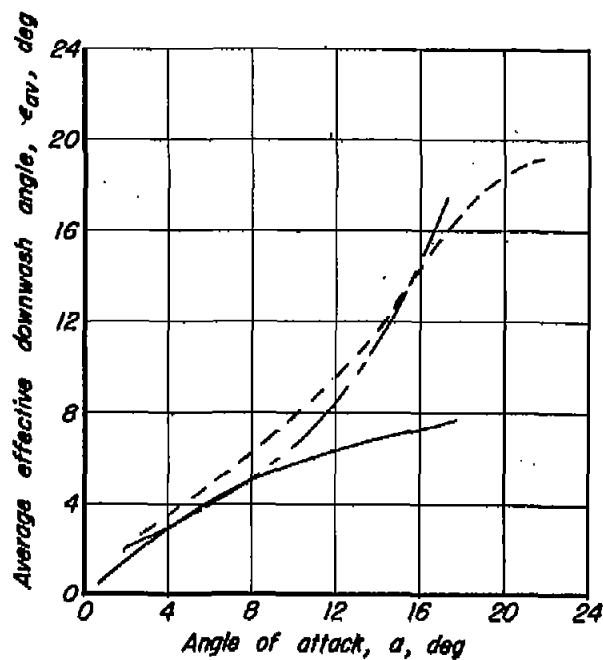
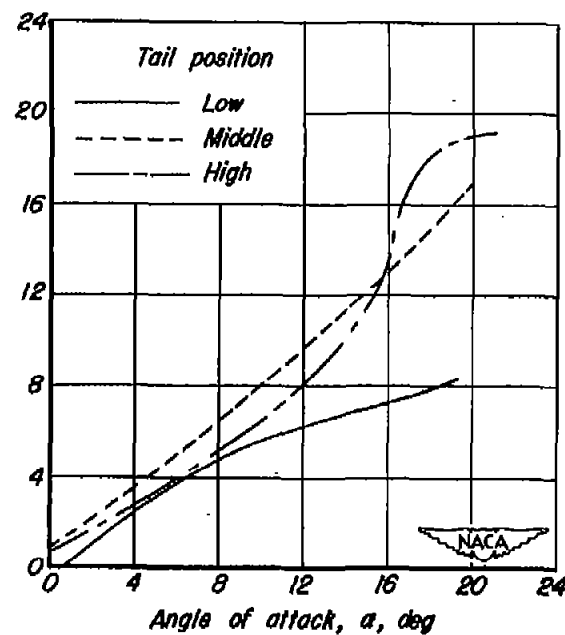
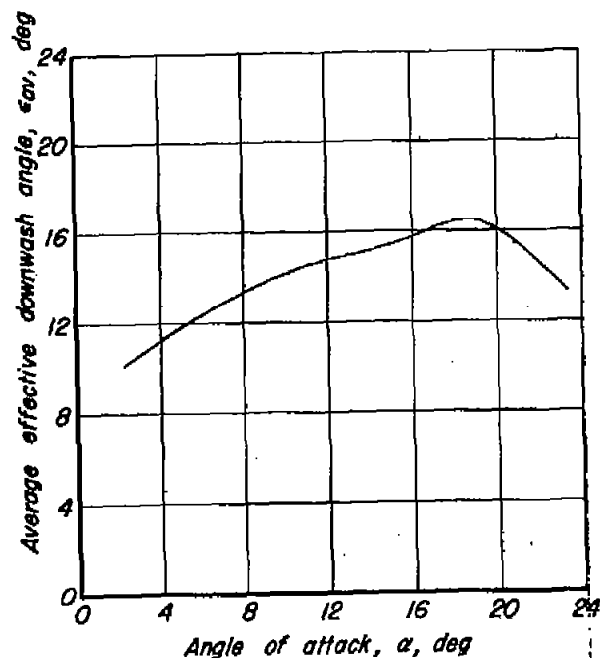
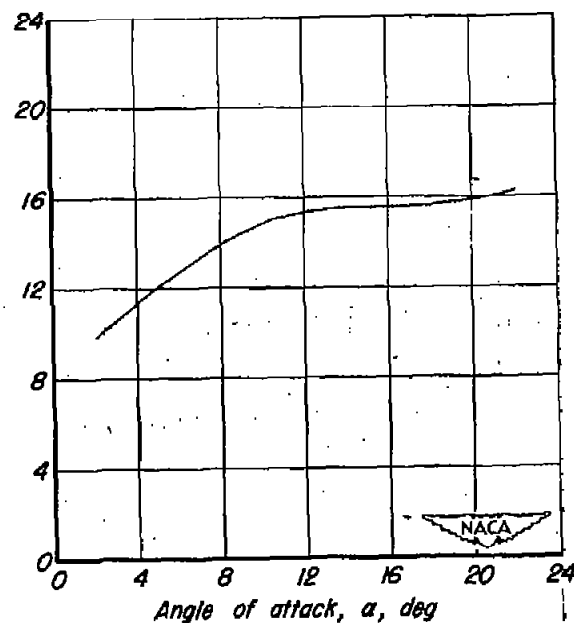
(a) $\lambda, 0.33$ (b) $\lambda, 0.20$

Figure 23.— Variation of average effective downwash angle at the horizontal tail with angle of attack; flaps undeflected.

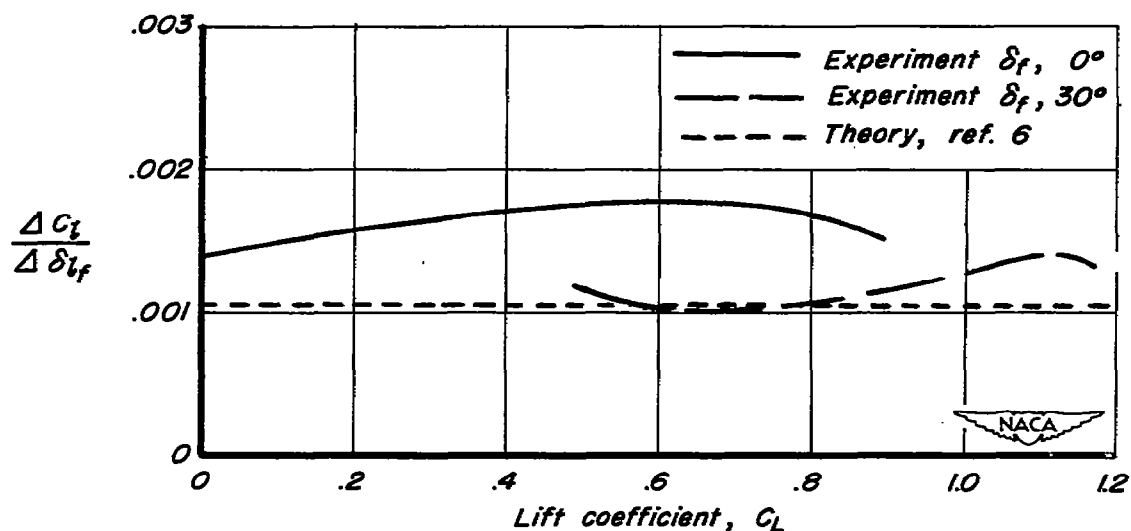


(a) $\lambda, 0.33$



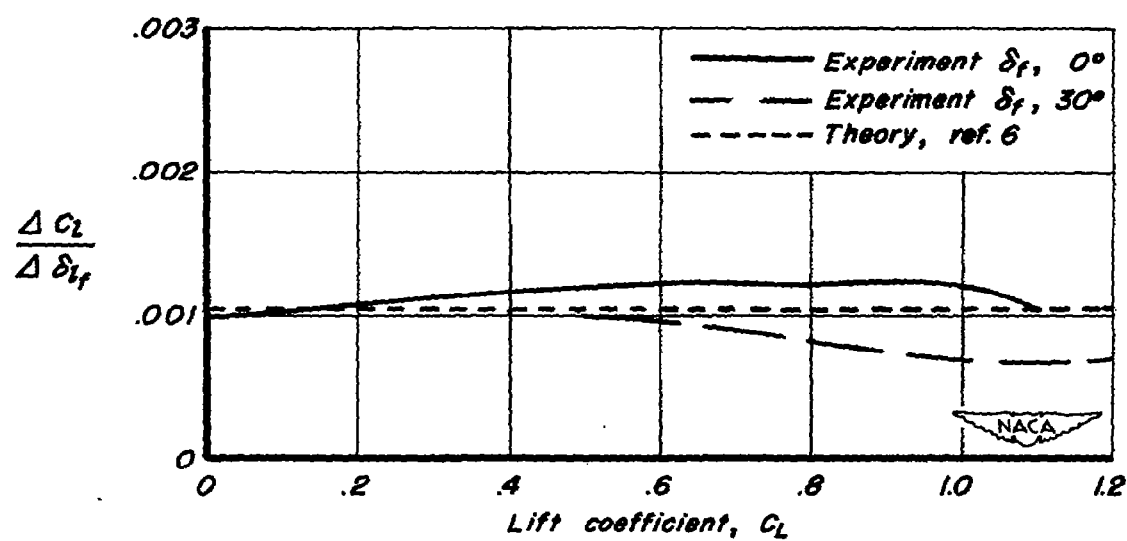
(b) $\lambda, 0.20$

Figure 24.— Variation of average effective downwash angle at the horizontal tail with angle of attack; flaps deflected to 40° and the horizontal tail in low position.



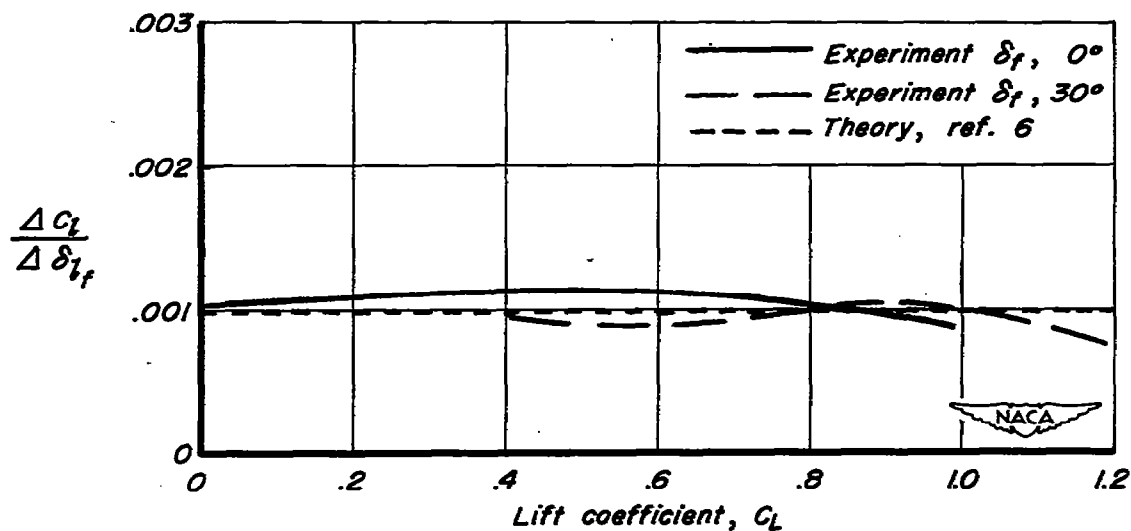
(a) Wing-fuselage vertical-tail configuration.

Figure 25.— The increments of rolling-moment coefficient per degree of differential flap deflection obtained by superposing a 10° antisymmetric flap deflection on two different flap settings for the model having a wing of taper ratio 0.33. $\delta_{l_f}, 20^\circ$; c.g., 0.338 \bar{c} .



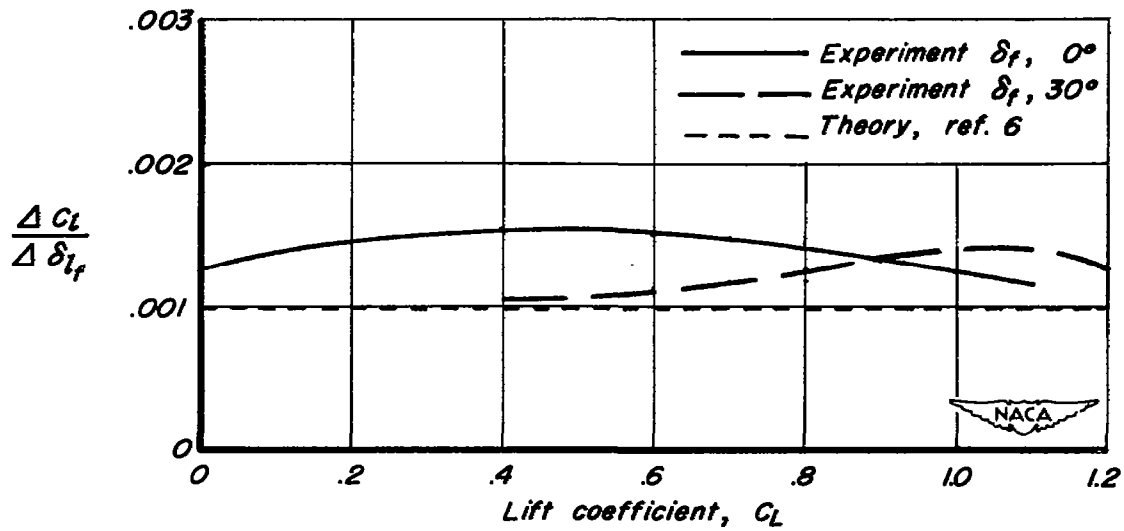
(b) Complete model. $i_f, -10^\circ$; $\frac{z}{b/2}, 0$.

Figure 25.— Concluded.



(a) Wing-fuselage — vertical-tail configuration.

Figure 26.— The increments of rolling-moment coefficient per degree of differential flap deflection obtained by superposing a 10° antisymmetric flap deflection on two different flap settings for the model having a wing of taper ratio 0.20. $\delta_{lf}, 20^\circ$; c.g., 0.369 \bar{c} .



(b) Complete model. $i_f, -6^\circ; \frac{z}{b/2}, 0.$

Figure 26.— Concluded.

NACA – Digidocs

Document processing error

Unreadable tiff image

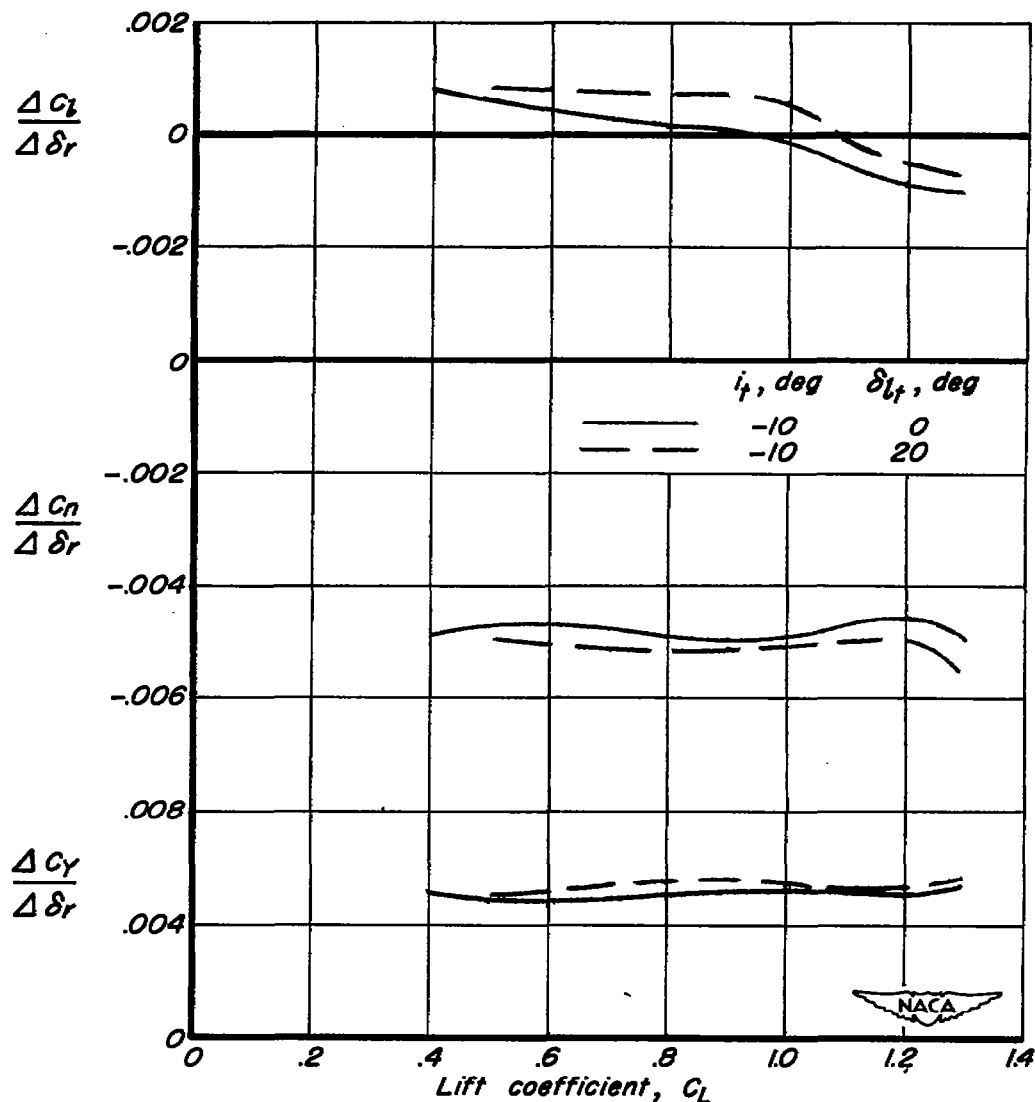


Figure 28.— Effects of an antisymmetric deflection of the horizontal tail on the rudder effectiveness of the model having a wing of taper ratio 0.33. $\delta_f, 40^\circ$; $\frac{z}{b/2}, 0$; c.g., $0.338\bar{c}$; $\delta_r, 10^\circ$.

SECURITY INFORMATION



3 1176 01434 8131

[REDACTED]

[REDACTED]